The Thesis Committee for Roya Alirezaei Abyaneh
certifies that this is the approved version of the following thesis:

Computational Modeling of Prestress Transfer, End-Region Cracks and Shear Behavior in Prestressed Concrete I-Girders Employing Large-Diameter Strands

APPROVED BY
SUPERVISING COMMITTEE:

Trevor Hrynyk, Supervisor

Oguzhan Bayrak, Co-Supervisor

Computational Modeling of Prestress Transfer, End-Region Cracks and Shear Behavior in Prestressed Concrete I-Girders Employing Large-Diameter Strands

by

Roya Alirezaei Abyaneh, BAppS

Thesis

Presented to the Faculty of the Graduate School of

The University of Texas at Austin

in Partial Fulfillment

of the Requirements

for the Degree of

Master of Science in Engineering

The University of Texas at Austin

August 2016

Acknowledgements

The love and care of my dearest Luca, Minoo, Hossein, Darya, Reza, Hengameh and many others motivated me over the course of this project. Their presence whether physical or on the phone, reminded me to be present and persistent.

I am indebted to Jessica Salazar, Alex Katz, Hyun su Kim, Dr. Hossein Yousefpour, my supervisors Dr. Trevor Hrynyk and Dr. Oguzhan Bayrak, and of course, the rest of the Ferguson laboratory family. The memories are endless and will be cherished forever.

I take this opportunity to acknowledge Dr. Hossein Yousefpour for his guidance, dedication and pursuit of quality which were the foundations of our research team.

I would like to express my sincere gratitude to Drs. Trevor Hrynyk and Oguzhan Bayrak for giving me the opportunity to contribute to this project. Dr. Hrynyk's constant support and encouragement and his expertise were fundamental in the development of my work.

Thanks to David Braley, Dennis Fillip, Blake Stasney, Michael Brown, Michelle Damvar, Deanna Mueller, Liz Clayton, John Bacon, Truman Oliver, Joel Arredondo, Jason's Deli and Austin's Pizza.

Abstract

Computational Modeling of Prestress Transfer, End-Region Cracks and Shear Behavior in Prestressed Concrete I-Girders Employing Large-Diameter Strands

Roya Alirezaei Abyaneh, M.S.E.

The University of Texas at Austin, 2016

Supervisor: Trevor Hrynyk,

Co-Supervisor: Oguzhan Bayrak

Prestressed concrete girders are commonly fabricated with 0.5-in. (12.7-mm) or 0.6-in. (15.2-mm) diameter prestressing strands. Recent interest in the use of larger (0.7-in. (17.8-mm) diameter) strands has been driven by potential benefits associated with reduction of the required number of strands and fabrication time, or potential increases in the workable range of prestressed concrete girders (i.e., greater capacities and span capabilities). A limited number of experiments on full-scale specimens with 0.7-in. (17.8-mm) diameter strands have shown that the load-carrying capacity and strand transfer length of specimens with 0.7-in. (17.8-mm) diameter strands can be conservatively estimated using existing AASHTO LRFD provisions. However, performance at prestress transfer requires further investigation to ensure that application of the strands with standard 2-in. (50-mm) spacing and conventional concrete release strength does not increase the end-

region cracking that is characteristic of prestressed girders. It must be verified that the development of such cracks does not stimulate anchorage-driven or premature shear failures prior to yielding of the shear reinforcement.

Previous research lacks in monitoring of reinforcement stresses and evaluation of end-region cracking which has long been a durability concern. A reliable finite element model that captures the behavior of the specimen at prestress transfer with consideration of performance from construction stages, over the course of the service life, and up to the ultimate limit state can provide key insight into the suitability of using of 0.7-in. (17.8-mm) diameter strands. Further, it could serve as an economical tool for the investigation and proposal of efficient end-region reinforcing details to reduce concrete cracking and enhance durability.

Finite element analyses of prestressed I-girder end-regions encompassing cracking and long-term creep- and shrinkage-induced damage, especially in girders fabricated with large diameter strands, have been limited. This research program assessed the limitations of 0.7-in. (17.8-mm) diameter strands at prestress transfer up to limit state response and investigated measures for enhancing the serviceability of the girders through finite element analyses using the commercial software, ATENA 3D. The finite element study was complemented with a full-scale experimental program which was used to validate the numerical results. This paper lays out a validated procedure for modeling the construction stages of prestressed girders and load testing. The model was then used as a tool for investigating alternative end-region reinforcement details for improved end-region serviceability. The most promising options are presented for consideration in further experimental studies and future implementation.

Keywords: ATENA 3D; large-diameter prestressing strands; prestress transfer; horizontal shear failure; prestressed concrete; 0.7-in.

Table of Contents

List of Tables

List of Figures

1. Introduction

The implementation of 0.7-in. (17.8-mm) diameter strands in prestressed concrete girders in place of the standard diameter strands (0.5-in. (12.7-mm) and 0.6-in. (15.2-mm) diameter) can reduce the number of strands required to obtain the required structural capacities. Alternatively, increased capacities and spans may be achieved by replacing the same number of standard strands with 0.7-in. (17.8-mm) diameter strands. Such benefits could facilitate construction efficiencies and/or increase the workable range of prestressed concrete girders. However, the limits associated with employing 0.7-in. (17.8-mm) diameter strands within the current standard concrete release strengths and strand spacing are yet to be investigated.

Two areas of concern associated with the introduction of large strands are: end-region serviceability and shear behavior. The end-regions of prestressed girders commonly develop cracks due to large stress concentrations in the concrete due to the transfer of the prestressing force from the strands to the concrete, via bond. Essentially doubling the prestressing force (i.e., by replacing fully stressed 0.5-in. (12.7-mm) diameter strands with 0.7-in. (17.8-mm) diameter strands) at the standard 2-in. (50-mm) spacing could intensify the concrete damage in the end-region. The potential development of larger width cracks stemming from this damage pose a greater risk of moisture and chloride penetration.

Severe cracking surrounding the strands may potentially lead to weakening of the strand anchorage and contribute to bond-related failures. Likewise, damage along the intercept between the flange and the relatively thin web of I-girders may stimulate horizontal shear failure (Hovell, et al., 2012). The applicability of such strands within the current AASHTO LRFD design guidelines needs to be investigated to ensure that the

serviceability requirements are met and that the transfer length and capacity of the girders can be conservatively estimated. From the limited full-scale testing that has been done on specimens with 0.7-in. (17.8-mm) diameter strands, it has been shown that the capacities of specimens constructed with 0.7-in. (17.8-mm) diameter strands can be conservatively estimated using AASHTO LRFD provisions. However, the present findings have been based on tests performed on specimens with unconventionally high concrete strengths at prestress transfer (Tadros & Morcous, 2011) or on specimens that were constructed with larger than standard strand spacing (Schuler, 2009). Additionally, much of the previous experimental research has been done with limited specimen instrumentation, making it difficult to assess the efficiency of the specimen designs (see Section 1.2).

The nature of distress in girder end-regions is very complex rendering an experimental investigation necessary to observe the effects of 0.7-in. (17.8-mm) diameter strands. A finite element model (FEM) of the girder with focused investigations of the end-regions can provide insight into the mechanics of prestress transfer, highlight critical stress patterns and identify the potential need for additional reinforcement. Thus, the FEM provides investigators with a method of optimizing reinforcement details and proposing economical solutions to be subsequently examined through additional experimentation.

ATENA 3D (ATENA), a commercial nonlinear finite element analysis (FEA) software, was used to model prestressed I-girders with 0.7-in. (17.8-mm) diameter strands. The models were validated and refined based on available experimental results from the literature. Various modified end-region reinforcement details were modeled in ATENA in four different prestressed girders and the most promising reinforcement details were recommended for subsequent experimental investigation. In addition to the end-region

investigation, analyses of the ultimate load tests performed on the specimens were used to investigate the failure modes observed.

This document presents the modeling approach, its validation and refinement based on experiments, and concludes with proposed reinforcement details to promote the serviceable implementation of 0.7-in. (17.8-mm) diameter strands in prestressed I-girders.

1.1 RESEARCH SIGNIFICANCE

A FEM of the end-region of prestressed I-girders which can capture the stress distribution in the anchorage zone facilitates the understanding of the complex stress conditions and also the development of effective reinforcement details for crack control.

The end-region response of prestressed I-girders reinforced with 0.7-in. (17.8-mm) diameter strands has not been investigated broadly in the literature, or in practice, in a way that captures the performance of specimens constructed using standard fabrication procedures and with consideration of long-term cracking. This paper lays out a modeling procedure using the commercial software ATENA 3D and describes the material models, assumptions, and boundary conditions which led to the development of a reliable FEM that was shown to successfully capture the response of prestressed I-girders employing 0.7-in. (17.8-mm) diameter strands. The FEM was used to predict the specimen behavior from prestress transfer to the ultimate limit state. Additionally, three end-region detailing modifications in four different prestressed I-girders were investigated and optimized for improved serviceability. The objectives of the study are:

1. Develop a practical and validated procedure for computer modeling of prestressed concrete I-girders (Chapter 2) to capture:

a. response at prestress transfer (e.g., concrete damage, transfer length and end-region reinforcement stresses);
b. load-deflection response under applied loads; and
c. failure modes governing the behavior at ultimate limit state.

2. Numerically estimate the behavior of actual prestressed beams available in the literature at prestress transfer and under applied loads (Chapter 3).
3. Employ the validated model to identify efficient reinforcement details to control undesirable end-region damage generated by high stress concentrations from large diameter prestressing strands (Chapter 4).

1.2 BACKGROUND

Upon the transfer of prestressing force from the strands to the surrounding concrete, three types of stresses are induced in the end-region of prestressed girders, namely: bursting, spalling, and splitting stresses. If the stresses are greater than the cracking strength of concrete at the time of release, cracks develop at characteristic locations in the end-region. Figure 1.1 demonstrates the primary locations of the cracks and their corresponding stress patterns.

Bursting cracks are prominent on the surface of the concrete along the location of the strands. They form as a result of tensile stress development perpendicular to the compression strut along the prestressed strands. Deep bursting cracks close to the strands can be particularly harmful for the durability of the girder (Okumus & Oliva, 2013).

Spalling cracks are characteristic of specimens with high eccentricity which is commonly the case in practice. Large prestressing eccentricity delivers an efficient design by maximizing the flexural capacity of the specimen. On the downside, eccentricity results

in the formation of longitudinal or diagonal cracks over the height of the web. Spalling cracks are the least critical of the types noted above as they occur the farthest away from the bottom strands. In some cases where the design requires top strands, spalling cracks near the top flange strands may become a concern. Figure 1.2 illustrates the deformation mechanism by which the cracks are formed. A typical pattern of surface end-region cracking is shown in Figure 1.3.

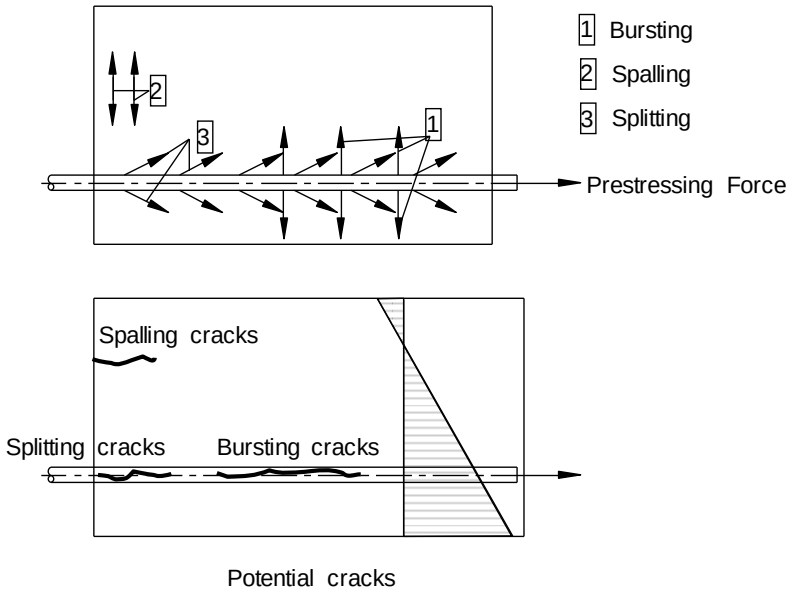

Figure 1.1: End-region stresses and potential cracks formed after prestress transfer (CEB, 1987)

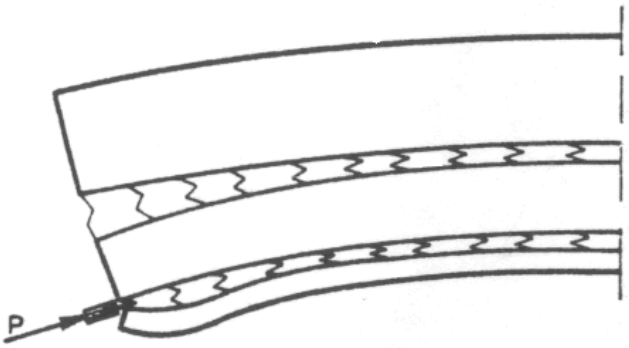

Figure 1.2: Exaggerated deformation mechanism of the end-region of prestressed beams (Lenschow & Sozen, 1965)

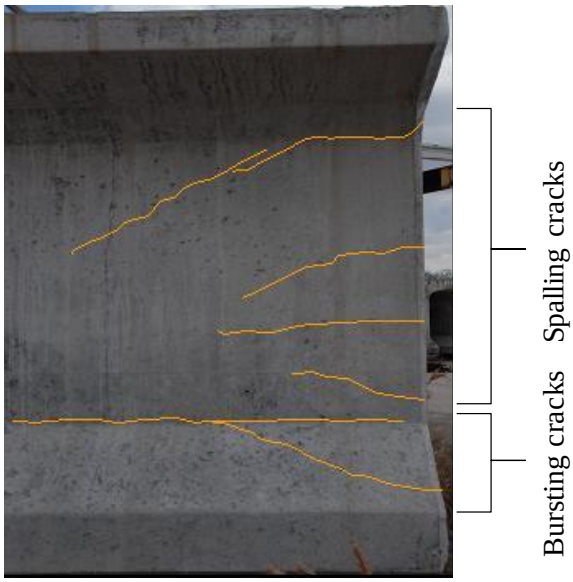

Figure 1.3: Typical bursting and spalling cracks in AASHTO Type VI Beams: Galveston Causeway Expansion Project (adapted from O'Callaghan (2007))

Splitting cracks may not be visible on the sides of the beam as they are formed around the strands as a result of radial compressive stresses. When strands are subjected to

tensile stresses, they elongate and reduce in diameter. At prestress transfer, they return back to their original diameter at the end face of a girder; thus exerting radial compressive stresses on their surrounding concrete. This response is commonly referred to as Hoyer's effect (Hoyer & Friedrich, 1939). Although not visible on the sides of the girder, splitting cracks may appear on the end faces and weaken anchorage. Repair of the end faces may be necessary for controlling moisture penetration.

To ensure durability of the precast prestressed girders, reinforcement is specified for the control of end-region stresses. This type of reinforcement is oriented in the transverse direction and is typically continued at least over a distance h, which is equal to the height of the specimen, away from each end of the specimen. Spalling reinforcement is placed in the web and bursting reinforcement is placed in the bottom flange enclosing the strands.

Prestressing strands are commonly placed on a standard grid of 2-in. (50-mm) horizontal and vertical spacing and are typically stressed to 75 % of their ultimate capacity (which equals 202.5 ksi (1396 MPa) for typical seven-wire Grade 270 strands by the ASTM A416 /A416 M standard.). The compressive strength of the concrete at release is typically in the order of 5 to 6 ksi (35-41 MPa). The introduction of 0.7-in. (17.8-mm) diameter strands at the given spacing and concrete compressive strength may contribute to increased stresses and concrete crack development as described in the following.

The prestressing forces applied to the strands are limited by maximum allowable stresses. The 2015 TxDOT LRFD Bridge Design Manual limits the maximum compressive stresses to $0.65 \cdot f'_{ci}$ (ksi) and the maximum tensile stress to $0.24 \cdot \sqrt{f'_{ci}}$ (ksi). In the case of 0.7-in. (17.8-mm) diameter strands, the allowable stresses (specified by the associated design code) remain the same as those permitted for girders constructed with 0.5-in. (12.7-

mm) and 0.6-in. (15.2-mm) strands. However, an increase in the strand diameter reduces the clear width of concrete between the strands. A greater magnitude of prestressing force per strand is applied on a smaller clear area of concrete (Figure 1.4). It is this magnification of stress at the strand level that has led to concerns regarding the severity of concrete cracking.

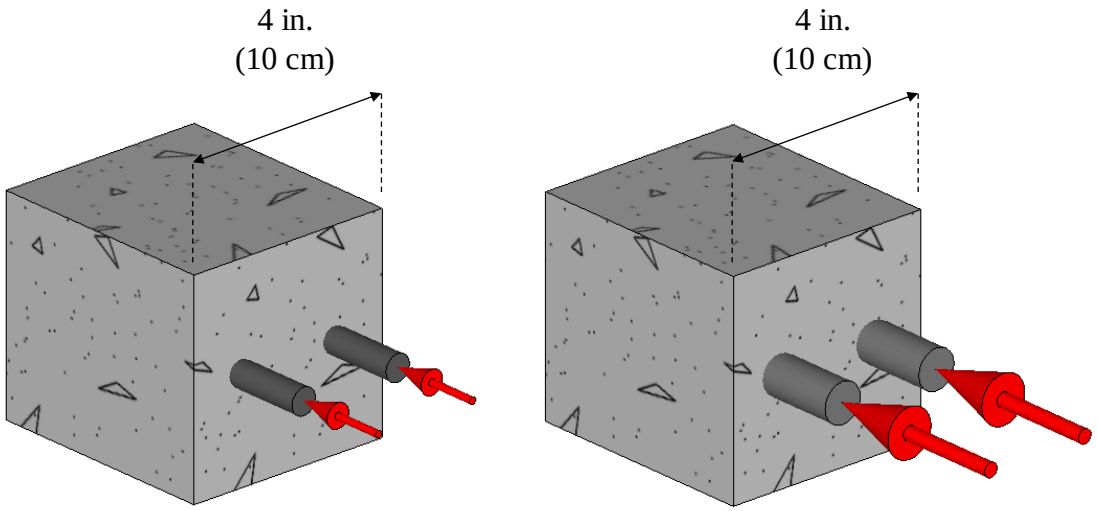

0.5-in. (12.7-mm) diameter strands
Force per strand: 31 kips (138 kN)
Applied pressure: 7.8 ksi (53 MPa)

0.7-in. (17.8-mm) diameter strands
Force per strand: 60 kips (265 kN)
Applied pressure: 14.9 ksi (103 MPa)

Figure 1.4: Intensification of prestressing force by using larger diameter strands

A number of studies have been conducted on the numerical analysis of the end-region behavior of prestressed I-girders to capture cracking and reinforcement stresses. The research is driven by concerns associated with cracks that permit moisture and chloride penetration. Fabricated girders are typically transported to the bridge and loaded, on

average, about 120 days after fabrication (Garber, 2014); meanwhile, creep- and shrinkage-induced strains further aggravate end-region cracks. Two measures, crack widths and steel stresses, have been used to assess and control the level of damage, respectively.

Okumus (2012) used the commercial software program Abaqus/CAE to investigate parameters influencing the latter in specimens comprising a testing program conducted on end-region behavior of prestressed I-girders (O'Callaghan, 2007). The focus of the research was on the development of a finite element model that would capture the short-term cracking formed by the transfer of prestressing from 0.6-in. (15.2-mm) strands in I-girders. In a 2013 paper, the long term growth of cracks in width and length were also investigated (Okumus & Oliva, 2013). The associated numerical analysis demonstrated that shrinkage strains contributed to crack growth as the stresses in the reinforcement decrease with time. In addition, it was also found that increasing the amount of reinforcement in the end-region was also estimated to increase the restraint on the concrete which, in turn, contributed further to the restrained shrinkage-induced cracks. The findings of the study suggested that it is best to increase the area of the reinforcement closest to the girder-ends as opposed to increasing the area of all end-region reinforcing bars. Although 0.7-in. (17.8-mm) diameter strands are suspected to generate larger stresses and damage, the findings of Okumus (2013) have important implications on the collaborative effects of reinforcement-induced concrete restraint and shrinkage in aggravating end-region cracking. To thoroughly assess the adequacy of recommended end-region modifications, it is important to consider specimens of different cross sections with varied levels of spalling and bursting stresses.

Ross (2014) tested various reinforcement details, in I-girders with 0.6-in. (15.2-mm) diameter strands, to reduce cracks in the end-region in an experimental study. This study did not consider long-term cracks, but concluded that increasing the area of

reinforcement in the end-region can reduce the cracks without deteriorating the shear capacity of the specimen. Other crack-mitigation methods considered in the study were strand debonding and post-tensioning of the end-region. Post-tensioning was shown to propagate diagonal web cracking under load-testing and thus, required further research for developing effective post-tensioning procedures. Strand debonding was shown to weaken bond and reduce the ultimate load-carrying capacity.

The research presented in the following chapters of this thesis serves to contribute to the improved serviceability of prestressed concrete I-girders employing 0.7-in. (17.8-mm) diameter strands through the development and application of a straight-forward finite element modeling approach done without the need for challenging material property assignment or analysis parameter definition (requirements typically associated with common FEA tools such as Abaqus) that is used to examine girder crack development for a variety of cross sections and prestress reinforcement conditions.

2. Numerical Modeling Approach

ATENA 3D (Červenka & Červenka, 2015) was used to perform all computational modeling described herein. This nonlinear FEA program was developed specifically for the analysis of reinforced concrete (RC) structures and operates within a three-dimensional graphical environment that can be used to display concrete cracking, crushing and reinforcement yielding by way of a graphical interface. A key feature of the numerical modeling approach employed was that the prestress transfer and member response under applied loads was considered using one only finite element model. Thus, the effect of concrete damage attributed to prestress transfer was considered in the subsequent assessment of the ultimate member behavior.

This chapter includes a summary of the techniques and assumptions used to develop the models developed in this document. Throughout the chapter, specific references are made to the specimens that have been analyzed. A summary of the specimens included in the present study is introduced in Table 2.1, and further discussion pertaining to each specimen is provided in Chapter 3. Note that the selected specimens presented in Table 2.1 correspond to specimens that were similar in geometry and concrete release strength to the Texas family of girders (Tx-Girders), and were reported with design details and test results that permitted accurate model development and interpretation. The NU1100 girders are standard I-girders that are fabricated for the Nebraska Department of Roads (NDOR). The Specimen IDs in Table 2.1 are annotated with the following format:

Strand diameter (in) • 10 – section size – identifier assigned by the researcher.

Table 2.1: Girder specimen analysis matrix

Specimen ID	Source	Tests
6-Tx28-I	O'Callaghan (2007), Avendaño (2008)	Prestress transfer, and shear
6-Tx28-II		
6-Tx46-I		
7-Tx46-I	Present Study	Prestress transfer, and shear
7-Tx46-II		
7-Tx70-I		
7-Tx70-II		
7-NU1100-I	Tadros & Morcous (2011)	Development length, and shear[1]
7-NU1100-II		
7-NU1100-III		

[1] Details regarding the performance under prestress transfer were not provided.

2.1 MESH DESCRIPTION

To minimize the computational effort required, all models were subdivided along their planes of symmetry. The specimen cross-sections were symmetric; however, the live and dead ends of most specimens had different reinforcement density, bond properties or were subjected to different loading configurations. Consequently, only half of the cross-sections were modeled; however, to accommodate changing details, full girder lengths were modeled for most specimens. Throughout this document, the X-axis, Y-axis and Z-axis correspond to the directions along the width, length and height of the specimens, respectively. The following figure shows the application of symmetry about the YZ plane. Note that other specimens with symmetric detailing over the lengths of the girders were also divided along the XZ plane at midspan.

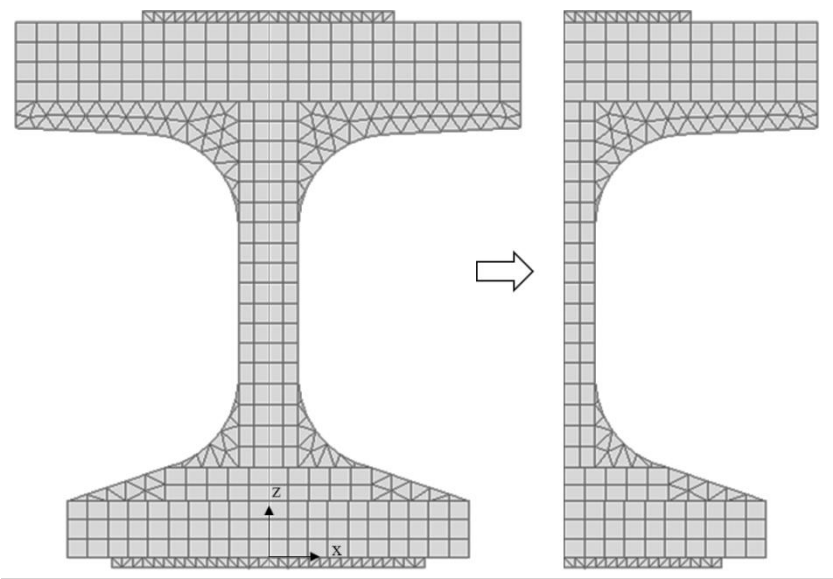

Figure 2.1: Finite element mesh of NU1100 girders

The model mesh and element sizing was consistent among all specimens and it was determined through an initial mesh sensitivity analysis which was conducted on 6-Tx28-I and 6-Tx28-II. Tx28 girders are 28-in. (710-mm) deep Tx-Girders and are the smallest specimen size considered in this analysis. The parameters examined in the mesh sensitivity study included the transfer lengths of the prestressing strands, crack patterns and crack widths resulting from prestress transfer.

A typical element size of 2.0 in. (50 mm) was used to model all regions of the specimen. In the case of the Tx28 cross-section, this resulted in approximately 16 elements through the depth. Further refinement of the mesh did not result in significant variations in the results for the key parameters of interest which consisted of the crack patterns, crack widths, transfer lengths and stirrup stresses. All other specimens described in this report had cross section that were larger than that of the Tx28 girders and were still modeled using 2.0-in. (50-mm) elements; therefore, greater mesh resolution was provided for larger

girders. Figure 2.1 illustrates the mesh density for a NU1100 girder that is 43-in. (1.1-m) deep. Figure 2.2 illustrates the mesh in a Tx70 girder with an 8-in. (20.3-in.) deep concrete deck, load- and bearing-plates.

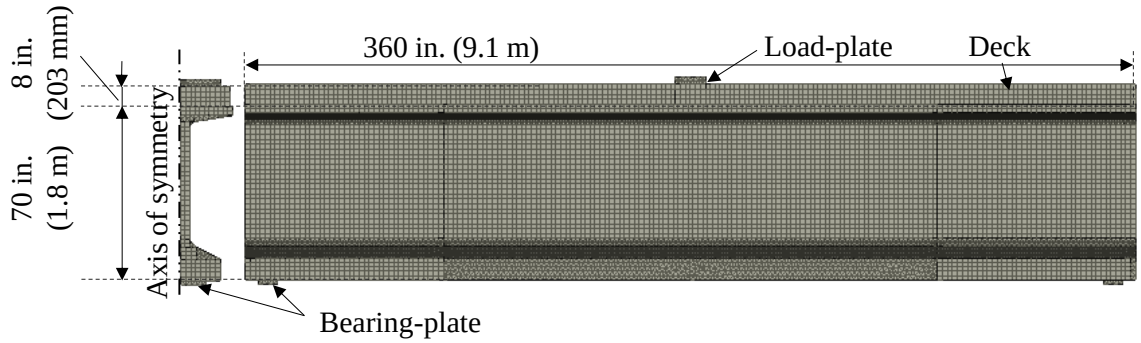

Figure 2.2: Finite element mesh of a Tx70 girder

ATENA provides 3D solid tetrahedral and brick elements with linear or quadratic interpolation functions for concrete. All models were constructed with brick elements with linear interpolation functions for concrete and 2D truss bar elements for the reinforcement. Tetrahedral elements were used in the flanges and all other areas where geometric restraints did not permit the use of rectangular brick elements.

2.2 LOAD CONDITIONS

This section summarizes the types of loads that were considered and the manner in which they were applied to simulate the loading conditions considered in the various testing programs.

2.2.1 Prestress Transfer

After a prestressed concrete specimen is cast and the design concrete release strength (f'_{ci}) is reached, the formwork is removed and the strands are released allowing the prestressing force in the strands to transfer to the surrounding concrete. The strands are released while the specimen rests on the soffit where it was initially cast. The self-weight of the specimen is supported by the continuous soffit prior to release of the strands. As a result of eccentric prestress force transfer, the specimen will typically develop some camber. The member's self-weight will play a role in opposing camber effects. This condition is descriptive of specimens that are simply-supported which applied to all specimens considered in the present study.

It is important to note that Červenka recommends that the self-weight and prestressing force be applied over the course of 10 load-steps, each step exerting only 10 % of the total load to maintain numerical stability (D. Pryl[1], e-mail communication, November 20, 2015). Thus, for all cases, the total girder self-weight was applied in the initial load step (i.e., step 1), and reinforcement prestrains were progressively increased to the desired level using twenty load steps. The convergence criteria and solution methods are described in Section 2.5.

The prestressing force is specified by the user; however, ATENA converts the specified force to an equivalent prestrain by way of the modulus specified for the strand material. The initial node of the strand represents the live end of the strand and the final node represents the dead end.

[1] Dr. –Ing. Dobromil Pryl is a consulting engineer at Červenka Consulting.

2.2.2 Intermediate Stage

After prestress transfer, the specimens were aged a minimum of 28 days prior to load testing. To capture the losses in the prestressing force with time as well as elongation and widening of release cracks, a volumetric strain of magnitude -0.2×10^{-3} in./in. was applied to the girder. This volumetric strain was meant to capture the losses induced by relaxation, shrinkage and creep that developed prior to the time of testing. During this aging period, the deck was cast and the specimen was transported to the test setup.

2.2.3 Ultimate Limit State Test

Because the primary focus of the present study was on girder shear behavior, all specimens considered in the analyses were subjected to shear-critical loading conditions. In the case of NU-Girders, first a "flexure" test was conducted followed by a "shear" test ((Tadros & Morcous, 2011). Table 2.2 and Table 2.3 list the load conditions considered for the Ultimate Limit State (ULS) tests.

Table 2.2: Shear-critical test loading conditions

Load Case	Load Type	Load Name	Step Size
1	Body load	Girder self-weight	100 %
2	Reinforcement prestrain	Prestressing force	5 %
3	Body load	Deck self-weight	100 %
4	Volumetric strain	Shrinkage	100 %
5	Prescribed displacement	Shear	0.01 in. (0.25 mm)

The ULS tests were modeled through the application of prescribed vertical displacement to a single node at the center of a load-plate. Each test program used load-plates to transfer the applied force from the rams to the specimens.

Table 2.3: Flexure-critical test followed by shear-critical test loading conditions

Load Case	Load Type	Load Name	Step Size
1	Body load	Girder self-weight	100 %
2	Reinforcement prestrain	Prestressing force	5 %
3	Body load	Deck self-weight	100 %
4	Volumetric strain	Shrinkage	100 %
5	Prescribed displacement	Flexure	0.01 in. (0.25 mm)
6	Prescribed displacement	Unload	
7	Prescribed displacement	Shear	

During the analyses of the flexure tests, the specimens were displaced to the experimentally reported displacement measured under the peak load. Next, a reverse displacement was used to subsequently unload. Note that due to plastic deformations, the net displacements of the girders were not zero after unloading. Following the unloading process, the specimen was loaded at the shear test loading location using a vertically prescribed displacement until failure of the girder. Section 3.3.2 describes that the FEM of NU-Girders failed during the first test as it was loaded to its shear capacity and the results of the second test were not beneficial and are not reported.

2.3 BOUNDARY CONDITIONS

The boundary conditions (BC) specified for the specimens were divided into two major groups: (BC2) conditions at the time of the ULS test setup (Load Cases 5-7) and (BC1) conditions before the test (Load Cases 1-4). Figure 2.3 summarizes the specimen's boundary conditions over the course of the analyses. This construction process was defined using the ATENA "Construction Cases" feature.

Table 2.4 lists the model components present at each stage and the corresponding BC.

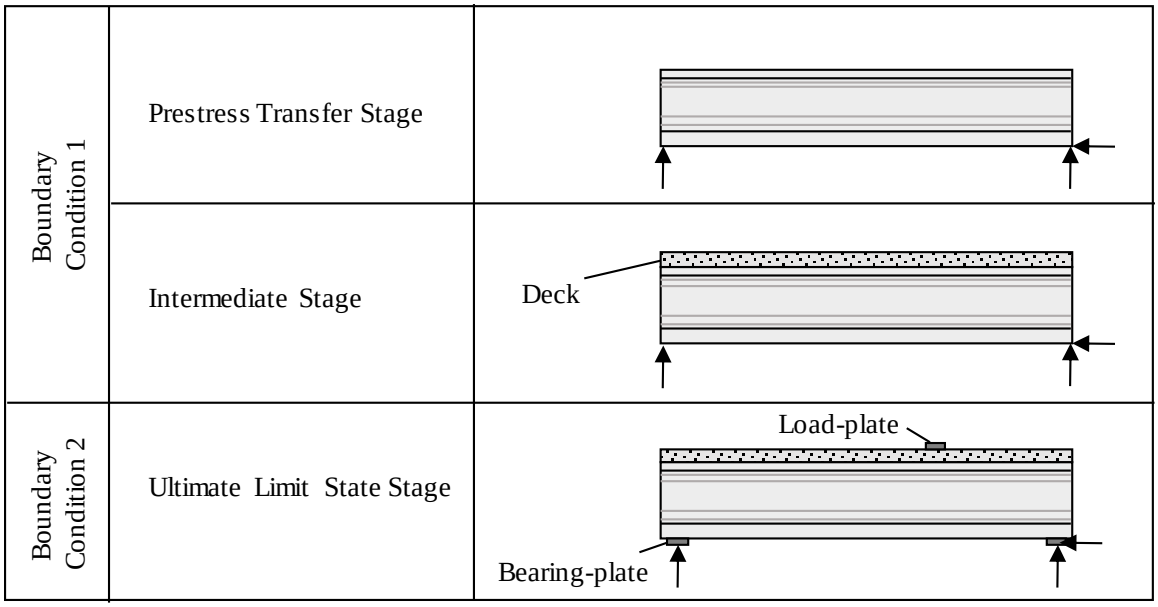

Figure 2.3: Overview of boundary conditions in all analyses stage

Table 2.4: Model component and BC summary

Load Case	BC ID	Load Stage	Components
1-2	1	Prestress transfer	Girder
2-4		Intermediate	Girder, deck
5-7	2	ULS test	Girder, deck, load and bearing-plates

As described in Section 2.2.1, the girder develops camber following prestress transfer. Camber forces the midspan of the girder to rise so that the girder is resting on its edges only rather than the entire soffit (see Figure 2.4). All planes of symmetry were translationally restrained in the directions normal to those planes. The vertical supports were modeled as either pins or rollers. In BC1, the dead end of a specimen was modeled as a pin whereas the live end was allowed to translate longitudinally. Figure 2.5 shows the details of the dead and live end restraints.

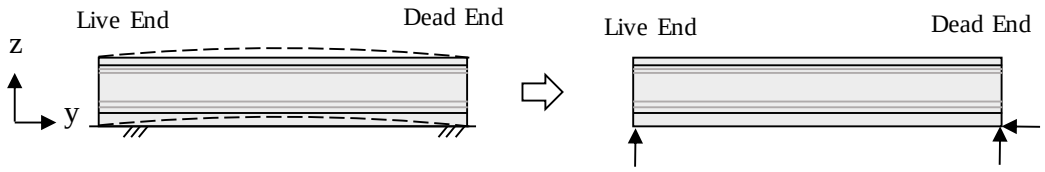

Figure 2.4: BC1 during the prestress transfer stage (elevation view)

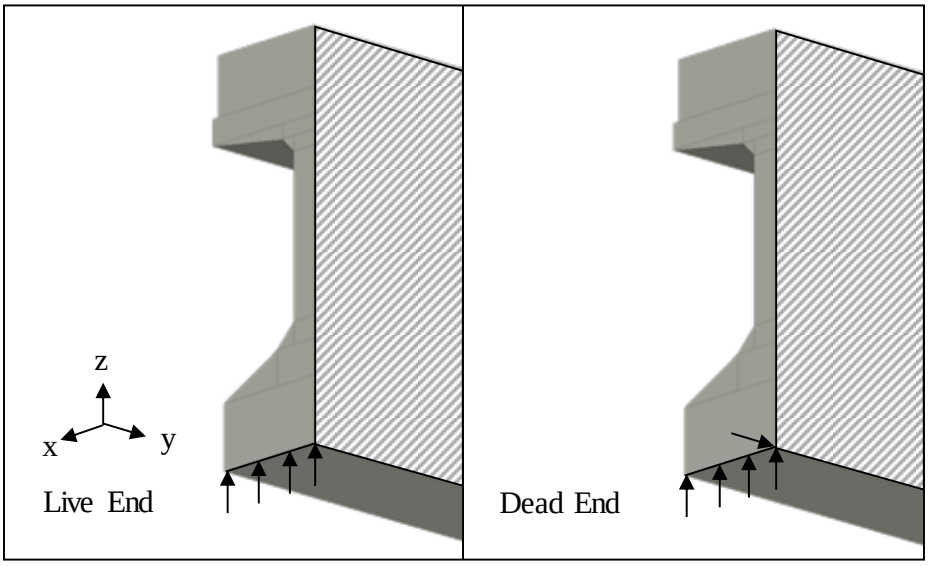

Figure 2.5: BC1 (isometric view). The hatched surface is the plane of symmetry restrained in translation perpendicular to the surface.

In BC2, the bearing-plates of the Tx-Girders with 0.6-in. (15.2-mm) strands were restrained from rotation as the plates were resting directly on larger concrete blocks. One bearing-plate was modeled to restrain longitudinal and vertical translations (similar to a pin) and the other to only restrain vertical translations (similar to a roller). The pinned-end was arbitrarily selected to be at the live end for the Tx-Girders with 0.6-in. (15.2-mm) strands. To restrain longitudinal translation in the pinned-end, a line at the center of the bearing-plate was restrained in the Y-axis. The bottom surface of each bearing-plate was restrained from vertical translation. The bearing-plates for the NU-Girders, and as well for

the Tx-Girders with 0.7-in. (17.8-mm) diameter strands, were allowed to rotate. To simulate the rotation, the bottom surface of the bearing-plates was restrained in the vertical direction only at the centerline of each plate. Figure 2.6 shows example photos taken of the actual supports in the test setups of Tx-Girders and NU-Girders and Figure 2.7 illustrates the ATENA simulation of the boundary conditions.

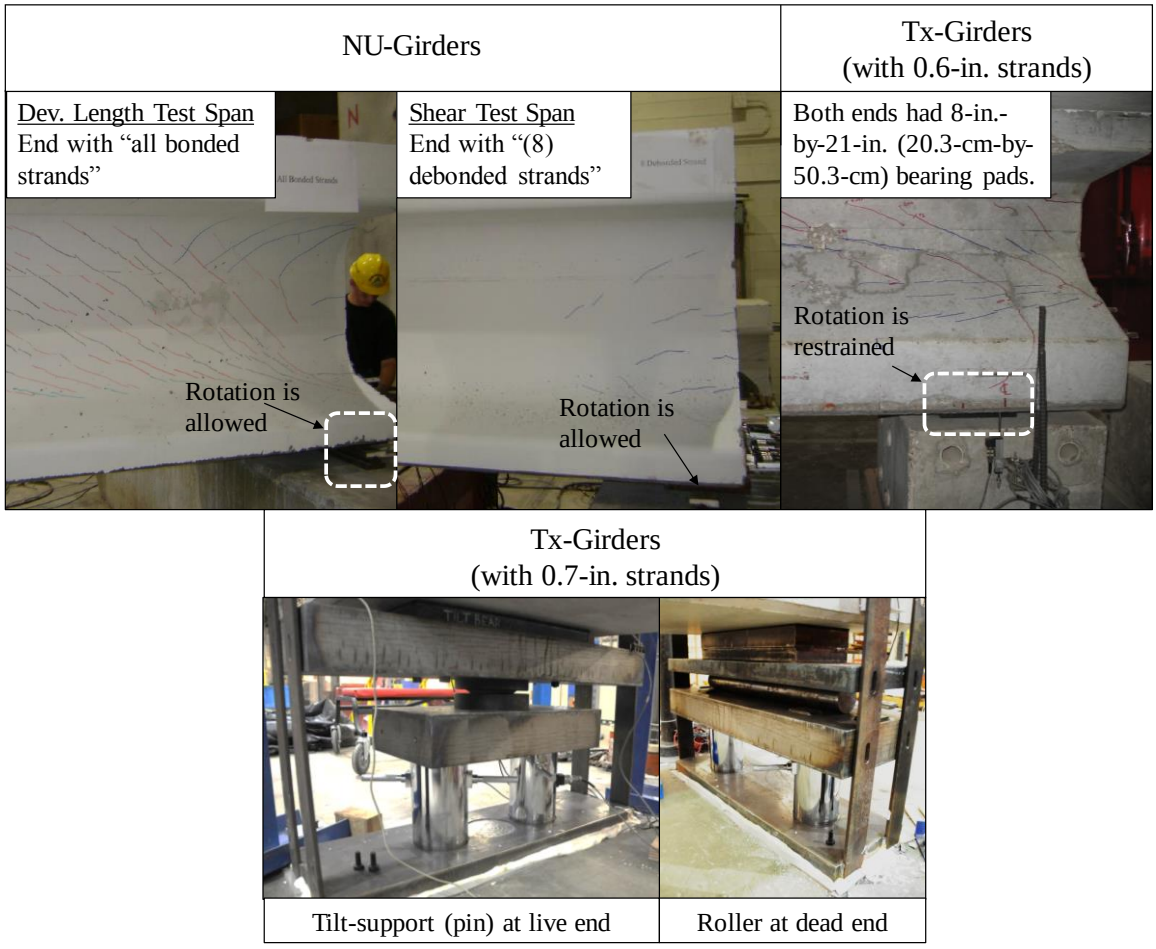

Figure 2.6: Bearing-plates. NU-Girders were resting on 3-in. (7.6-cm) thick plates on top of rollers (adapted from Tadros & Morcous (2011) and Avendaño (2008)).

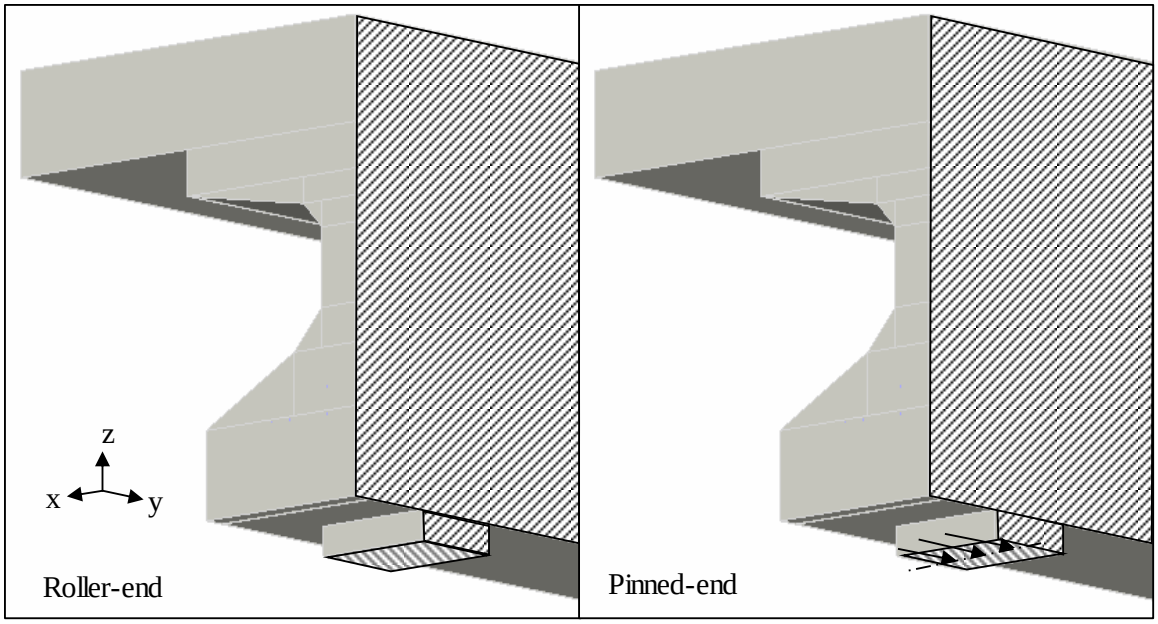

Figure 2.7: Boundary conditions during the ULS test stage (isometric view). The hatched surfaces are restrained in translation perpendicular to the surface. In the case of NU-Girders, the bottom surface of the bearing plate is only restrained vertically along its centerline.

2.4 BEHAVIORAL MODELS

Six materials types were defined in the modeling of members comprising the present study: deck concrete, girder concrete, conventional reinforcement steel, prestressing steel and welded wire reinforcement steel. In cases where measured material properties were available, they were used to define the material models; in all other cases, default material properties proposed by ATENA were used. This section reports the material properties and Chapter 3 provides the reinforcement detailing for each specimen. The reinforcement bond properties are also defined as "material" models in ATENA and are described in this section.

2.4.1 Conventional Reinforcing Steel

Reinforcing bars may be modeled discretely or as smeared reinforcement with perfect bond or a bond model. All reinforcing bars were modeled with perfect bond and as discrete bars so that strain gage data can be directly compared with the computed strains in ATENA. Material properties were known only for the Tx-Girders. Tadros & Morcous (2011) indicated that Grade 60 steel was used for conventional reinforcement without reporting mechanical properties. Chapter 3 provides material properties for each specimen. Figure 2.8 illustrates the stress-strain (σ–ε) relationships used. Where measured data were available, the "Multilinear model" was used which allows specification of several data points. Otherwise, the "Bilinear with hardening model" was used based on ASTM standard modulus, yield and rupture strengths.

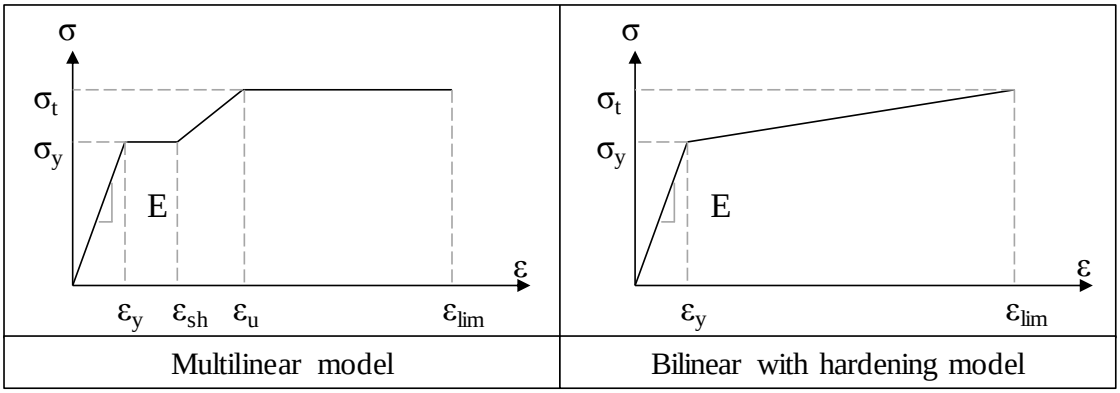

Figure 2.8: Stress-strain relationship used for conventional reinforcement (adapted from ATENA3D)

2.4.2 Prestressing Steel

Prestressing strands were modeled as discrete reinforcement with the prestressing force applied as a load case (see Section 2.2.1). To define the cross-section of a strand, an equivalent circle diameter was specified so that the area of the modeled strand equaled the actual area of the seven-wire strand. ATENA automatically calculates the perimeter of the strand based on this equivalent diameter. The difference between the actual perimeter and the calculated perimeter was assumed to be negligible. Measured material properties of prestressing steel were available for all Tx-Girders. Tadros & Morcous (2011) provided the strand material properties from two producers in detail; however, it was not indicated which producer's products were used in the construction of the NU1100 girders. Therefore, average material properties from the two producers were used. Chapter 3 provides the available strand material properties of each specimen.

2.4.3 Welded Wire Reinforcement Steel

Welded wire reinforcement (WWR) was used in some specimens, only. Chapter 3 summarizes the WWR material properties for specimens reinforced with WWR.

2.4.4 Prestressing Strand Bond Model

The prestressing force in the strands is transferred to the surrounding concrete through the bond between the two materials. In order to capture the transfer length and accurately predict the damage observed at the time of prestress transfer, a bond model was defined for the strands. The ATENA material library includes two bond models: CEB-FIB Model Code 1990 (CEB-FIP, 1993) and Bigaj (1999). Each model was based on a variety of different factors including the strand diameter, surface roughness of the reinforcement, surrounding concrete strength, level of confinement, and the quality of the bond. Bigaj

(1999) with "very good" bond quality was found to be the model that best captured the transfer length and the observed girder damage at prestress transfer. This selection was made after comparing the results of all bond model configurations with the measured data available from the prestress transfer in 6-Tx28-I, 6-Tx28-II, 6-Tx46-1 and another 6-Tx70-I girder. 6-Tx70-I was not included in the analysis matrix as a shear test report was not available.

The bond model properties were kept constant during the analysis; however, in reality, the concrete strength is typically believed to affect bond, and there was often considerable concrete compressive strength gain from the time of the prestress transfer stage to the time of member ULS test. To account for this variation, the bond model during the prestress transfer stage analysis was based on the concrete release strength, f'_{ci}, but for the analysis of specimens under ULS tests, the prestress transfer analysis was repeated from the initial step, with the bond model based on the concrete strength on test day. This solution was an approximation made to account for stronger bond and greater engagement of the strands during the ULS tests. When the analysis was repeated with the greater bond strength from the initial stage, the concrete damage at prestress transfer may increase slightly as relatively less energy was dissipated by strand slip. The downfall of this approximation for the ULS test was that the increased concrete damage from the prestress transfer stage may slightly influence damage during the ULS tests. Regardless, the ULS responses of the specimens considered in the validation studies were predicted well using this procedure.

2.4.5 Concrete

The concrete constitutive model in ATENA is based on a fracture-plastic model and considers geometric nonlinearity. The ATENA material library contains three concrete material models: "NonLinearCementitious", "NonLinearVariableCementitious", and "NonLinearCementitiousUser".

The constitutive model for all three options combines tensile (fracture) behavior and compressive (plastic) behavior models into a fracture-plastic model (Červenka, 2014). The "NonLinearCementitiousUser" model parameters are defined by the user, whereas the "NonLinearVariableCementitious" model was defined by ATENA and it allows the user to input different properties for each analysis step. Both the "NonLinearVariableCementitious" and "NonLinearCementitious" models require the user to specify the concrete cube compressive strength, at a minimum. Based on the user-specified strength, all other parameters can be generated automatically. The user has the choice of modifying them, but it is important to note that the default parameters produced good results based on the validations carried-out through this work (see Chapter 3); therefore, default parameters were used in all cases.

The two stages of specimen response that were of greatest importance in the analyses were prestress transfer and performance under applied shear. These two stages take place at different concrete strength levels. ATENA was especially useful as it supported the variation of the concrete material with each analysis step.

Deck Concrete

Since the deck concrete contributes to member response only during the ULS test, there was no need to capture the variation of its compressive strength. The deck concrete

material was modeled with the strength measured on the day of the ULS test using the "NonLinearCementitious" model.

Girder Concrete

The material model chosen for the girder accounted for the variation in material properties. The concrete model was based on f'_{ci} at the prestress transfer stage and on f'_c at the ULS stage. For this purpose, the "NonLinearVariableCementitious" model was chosen. With this model, the user may define certain variable parameters for each step of the analysis. However, there are other parameters that remain constant during the analysis and are automatically generated based on the f'_{ci} magnitude. The user may modify them; however, they will not vary during the analysis. Table 2.5 lists the variable parameters and the constant parameters. Some of the parameters are not automatically considered by default; however, the user may activate them.

Some of the automatically calculated parameters that remain constant during the analysis are not visible in the user interface. They may be viewed in the input file of the model. To ensure that all constant properties resemble the test day concrete properties, it is recommended to create the concrete material model based on the test day strength then modify the variable properties to account for the prestress transfer analysis steps.

By default, there is no tension stiffening in the model; however, tension stiffening with a magnitude of 5 % of the cracking stress was assigned for improving numerical stability after cracking. In addition, the plastic strain at compressive strength, $\varepsilon_{cp,}$ which is used in the constitutive model to calculate crack widths is automatically calculated based on the first concrete strength specified by the user. The value must represent the plastic strain at compressive strength based on the test day concrete compressive strength.

Table 2.5: Girder concrete material model parameters

Parameter Type	Parameter	Value	Active-by-default (Y/N)
Basic	Elastic modulus, E	Variable	Y
	Poisson's ratio, μ	Constant	Y
	Tensile strength, f'_t	Variable	Y
	Compressive strength, f'_c	Variable	Y
Tensile	Specific fracture energy, G_F	Variable	Y
	Crack spacing, s_{max}	Constant	N
	Tension stiffening	Constant	N
	Unloading	Constant	N
Compressive	Critical compressive displacement, W_d	Constant	Y
	Plastic strain at compressive strength, ε_{cp}	Constant	Y
Miscellaneous	Failure surface eccentricity	Constant	Y
	Multiplier for the plastic flow dir., β	Constant	Y
	Specific material weight, ρ	Constant	Y
	Coefficient of thermal expansion	Constant	Y
	Fixed crack model coefficient	Constant	Y

2.5 SOLUTION METHODS

ATENA offers two solution methods to perform the load-stepping analysis: Newton Raphson and Arc Length. Since the test loads were applied through prescribed displacements, the Newton Raphson solution method was deemed more suitable (Červenka, 2014). The convergence criteria and iterative procedure were modified to ensure adequate convergence was obtained over the course of the analyses, as listed in Table 2.6.

Table 2.6: Modified Newton Raphson solution method parameters

Parameter		Modification
General	Update stiffness	Each step
	Stiffness type	Elastic
	Iteration limit for one analysis step	80
Conditional Break Criteria (Break after step)	Displacement error multiple	10
	Residual error multiple	10
	Abs. residual error multiple	10
	Energy error multiple	1000

2.6 ASSUMPTIONS

As described earlier, a number of assumptions were made in establishing suitable material properties/behavioral models and analysis methods. The following provides a brief overview of the assumptions common to all specimens. Assumptions that are specific to each specimen are described in Chapter 3.

- The bond model for the ULS test analysis was developed based on test day concrete compressive strength. Since the bond model is constant throughout the analysis, the accuracy of the concrete damage computed at the prestress transfer stage may suffer. It was assumed that the difference in concrete damage would not alter the ULS results significantly.
- All non-prestressed reinforcing bars are perfectly bonded with the concrete.
- The bottom surface of the deck and the top surface of the girder are perfectly bonded (no interfacial slip can occur).
- The effect of deck shrinkage was neglected.
- Where Grade 60 steel mechanical properties were not available, standard values were obtained from the ASTM standard A615.

- WWR properties for the NU-Girders were adapted from earlier tests on WWR conducted by Tadros et. al. (Amorn, Girgis, Bowers, & Tadros, 2007). The mechanical properties adapted are averages values developed from the three different material suppliers considered in the research program.
- The response of the specimens attributed to transporting the specimens from the prestressing bed to the loading frame was neglected. Note that Okumus (2013) reported that lifting of the specimens following prestress transfer can increase end-region cracking.

3. Validation Studies

Prior to employing ATENA for simulating the behaviors of I-girders with large diameter strands, the prediction capabilities of ATENA were assessed using a series of experimental results from the literature. The modeling procedure described earlier yielded good agreement between the analytical and experimental results as presented in this chapter. With the developed modeling approach, the end-region stresses were thoroughly investigated, and measures to control damage and potentially even mitigate anchorage or horizontal shear failures were evaluated (see Chapter 4).

Two stages of specimen response were of interest for the present study: prestress transfer and shear resisting performance. From the relevant prestressed I-girder studies available in the literature, girders with concrete release strengths close to the TxDOT maximum allowable strength of 6.0 ksi (38 MPa) and standard 2-in. (5-cm) strand spacing (TxDOT, 2015) were selected for the validation studies (see Table 2.1).

Three of the specimens were I-girders with 0.6-in. (15.2-mm) strands fabricated in 2007 and tested at FSEL to investigate the tensile stresses in the end-regions (O'Callaghan, 2007) and the shear behavior (Avendaño, 2008) of TxDOT prestressed I-girders. The latter experiments were of particular interest for the documentation of end-region damage caused by prestress transfer, in addition to the observation of horizontal shear failure modes. Three other specimens were selected from the only available experimental study involving the shear behavior of full-scale prestressed I-girders with 0.7-in. (17.8-mm) diameter strands (Tadros & Morcous, 2011). It is important to note that the concrete release strengths of these specimens were unconventionally high, but in comparison to other specimens provided in the literature, were most similar to the current TxDOT standard of 6.0 ksi (38 MPa).

The crack patterns, crack widths, transfer lengths and stirrup stresses were the parameters of greatest interest in the release test numerical validation studies. The load-deflection responses and the failure mechanisms were key parameters of interest in the shear test validations. An overall assessment of the validation studies indicated that ATENA could adequately capture the damage induced by prestress transfer during the release experiments and could estimate distinct bursting and spalling cracks. As for the shear tests, the stiffness and failure mode were captured accurately. This chapter provides a summarized description of the six validated models. Finally, the methodology used to analyze Tx-Girders fabricated with 0.7-in. (17.8-mm) diameter strands is discussed.

3.1 TX-GIRDERS WITH 0.6-IN. (15.2-MM) STRANDS (O'CALLAGHAN; AVENDAÑO)

Three 30-ft long prestressed Tx-Girders with 0.6-in. (15.2-mm) diameter strands were fabricated at FSEL to study end-region stresses and develop end-region reinforcement details for the purpose of controlling release-induced cracks and stirrup stresses (to less than 20 ksi) in prestressed I-girders. One specimen, identified as 6-Tx46-I, was cast prior to the findings of O'Callaghan, and its reinforcement detailing was based on the TxDOT standard of 2007. The other two specimens (6-Tx28-I and 6-Tx28-II) were fabricated based on reinforcement details developed by O'Callaghan. The Appendix compares the end-region reinforcement design with the then-current provisions from AASHTO LRFD Bridge Design Specifications (2007), PCI Design Handbook (6th Edition) Guidelines and CEB-FIP Model Code 1990 Provisions.

The same girders were subsequently loaded monotonically to failure to study their shear resisting behavior (Avendaño 2008). Both the release and shear test results were used in the ATENA validation studies. Each end of each specimen was individually tested under

shear, resulting in two shear tests performed for each beam; however, given that the results from the two tests were shown to be highly consistent, only the first test performed on each specimen was considered for verification.

All of the Tx-Girders were fabricated with four 0.5-in. (12.7-mm) diameter strands in the top flange, each prestressed to 5 kips (22 kN). Table 3.1 summarizes the specimen design and test setup information. The specimen end corresponding to the second test, which was not modeled, is identified by "NA". Figure 3.1 shows a typical Tx-Girder. Figure 3.2 and Figure 3.3 illustrate the test setups used.

Table 3.1: Specimen and test setup detail of Tx-Girders with 0.6-in. (15.2-mm) strands

		Specimen	6-Tx28-I		6-Tx28-II		6-Tx46-I	
		End	Live	Dead	Live	Dead	Live	Dead
Test Setup		Beam Length	30 ft (9.1 m)					
		Span Length	28 ft (8.5 m)				28.5 ft (8.7 m)	
		Shear Span Length	NA	7 ft (2.1 m)	9 ft (2.7 m)	NA	10 ft (3.1 m)	NA
		a/d_p	NA	2.9	3.8	NA	2.7	NA
Transverse Reinforcement		Stirrup Type	Standard		WWR			
		Stirrup Spacing (2)No. 4 [in. (cm)]	1@2.5 (6.4), 4@3 (7.6), 8@4 (10.2), r@12 (30.5)	1@2.5 (6.4), 12@4 (10.2), r@12 (30.5)	1@2.5 (6.4), 12@4 (10.2), r@12 (30.5)	1@2.5 (6.4), 4@3 (7.6), 8@4 (10.2), r@12 (30.5)	1@2.5 (6.4), 4@3 (7.6), 8@4 (10.2), 4@6 (15.2), r@12 (30.5)	1@2.5 (6.4), 12@4 (10.2), 4@6 (15.2), r@12 (30.5)
		Measured F_y [ksi (MPa)]	65 (448)		75 (517)			
		Extra (2) No. 6 [in. (cm)]	1@1.9 (4.8), 3@3 (7.6)	1@1.9 (4.8), 3@4 (10.2)	1@1.9 (4.8), 3@4 (10.2)	1@1.9 (4.8), 3@3 (7.6)	1@1.9 (4.8), 3@3 (7.6)	1@1.9 (4.8), 3@4 (10.2)
		Measured F_y [ksi (MPa)]	65 (448)					
Concrete		Girder f'_{ci} [ksi (MPa)]	10 (69)		6.5 (45)		6.5 (45)	
		Girder f'_c [ksi (MPa)]	13.8 (95)		11.4 (79)		13.2 (91)	
		Deck f'_c [ksi (MPa)]	5.1 (35)		6.5 (45)		6.8 (46)	
		Deck Dimensions (width-by-thickness)	6-ft-by-8-in. (1.8-m-by-0.2-m)				3-ft-by-8-in. (0.9-m-by-0.2-m)	
Strands		Measured F_y [ksi (MPa)]	245 (1,689)					
		Measured F_u [ksi (MPa)]	285 (1,965)					
	Bot	A_{ps} [in.^{2} (cm^2)]	7.8 (50.4)				9.6 (61.7)	
		f_{pi}[ksi (MPa)]	205 (1,413)		218 (1,503)		203.5 (1,403)	
		e_{ps} [in. (cm)]	5.3 (13.4)				11 (27.9)	
	Top	A_{ps} [in.^{2} (cm^2)]	0.9 (5.6)					
		f_{pi} [ksi (MPa)]	23 (159)					
		e_{ps} [in. (cm)]	13.5 (34.3)				24.4 (62)	

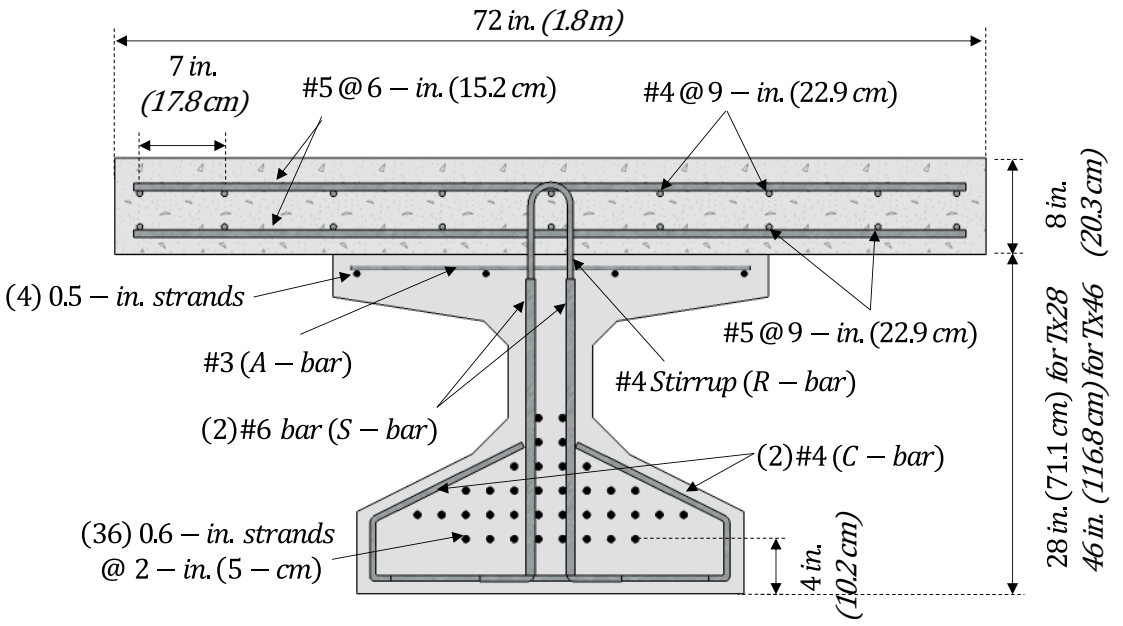

Figure 3.1: Cross-section and reinforcement details of Tx-Girders with 0.6-in. (15.2-mm) strands

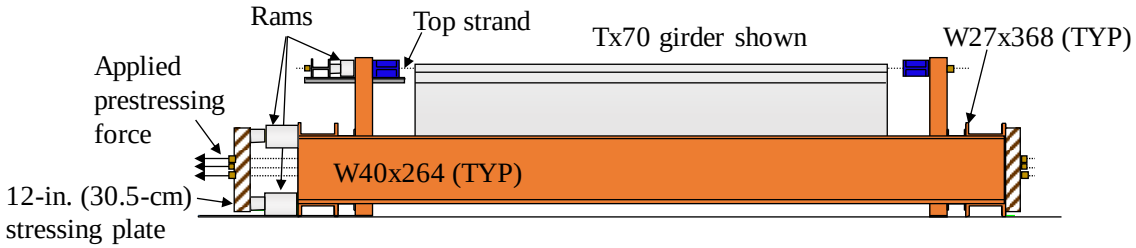

Figure 3.2: Release test setup of Tx-Girders with 0.6-in. (15.2-mm) strands (elevation view of prestressing bed) (adapted from O'Callaghan (2007))

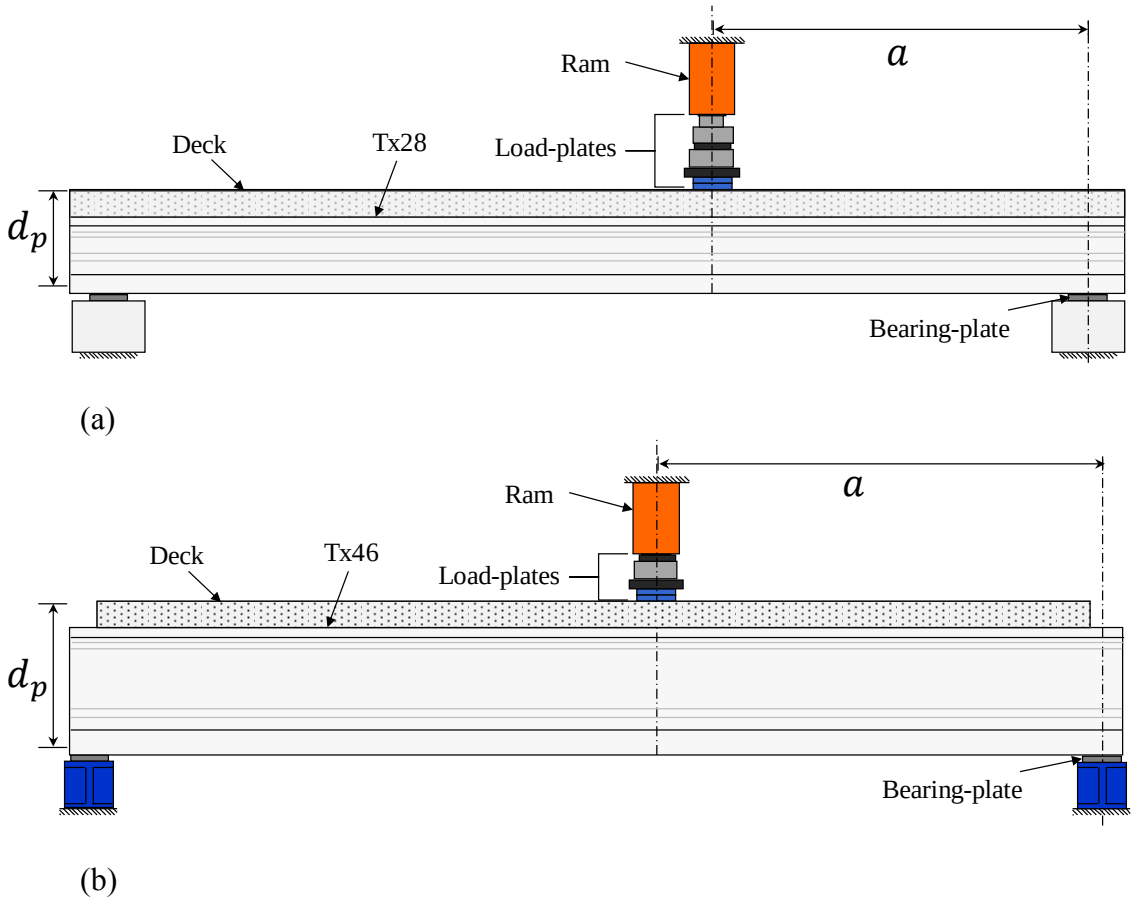

Figure 3.3: Shear test setup of Tx-Girders with 0.6-in. (15.2-mm) strands (elevation view) (a) Tx28 girders (b) 6-Tx46-I

3.2 NU-GIRDERS WITH 0.7-IN. (17.8-MM) DIAMETER STRANDS (TADROS & MORCOUS)

Tadros & Morcous (2011) studied the application of 0.7-in. (17.8-mm) diameter strands in different standard NDOR prestressed girder shapes. As mentioned earlier, only three 40-ft (12.2-m) long girders from this experimental program were deemed as being directly relevant to the present study. The three girders considered were fabricated at CoreSlab Structures, Inc. (Omaha), with different confinement reinforcement details in an effort to assess the effectiveness of standard reinforcement detailing on the bond development of 0.7-in. (17.8-mm) diameter strands. The experiments were conducted at the

Peter Kiewit Institute (PKI) laboratory in Omaha, Nebraska. The selected specimens (standard NDOR I-Girders called NU-Girders) were 43-in. (1.1-m) deep and are referred to as NU1100. They were fabricated with four 0.5-in. (12.7-mm) diameter strands in the top flange, which were fully prestressed to 30.9 kips (138 kN). Table 3.2 shows the variation in the confinement reinforcement detailing used amongst the specimens. Figure 3.4 and Figure 3.5 show the cross-section geometry and reinforcement detailing of the girders.

No observations were reported from prestress transfer; instead, a flexure-critical and a shear-critical test were performed sequentially on opposite ends of each specimen. The objective of the flexure-critical (development length) test was to ensure that 0.7-in. (17.8-mm) diameter strands can be developed at the AASHTO predicted development length of 14 ft (4.3 m). This test was conducted by monotonically loading the specimens at an a/d_p ratio of 3.4, 14 ft (4.3 m) from one end. The specimens were loaded just beyond their estimated nominal flexural capacities, then unloaded.

Table 3.2: NU1100 confinement reinforcement details

Girder	Specification	Confinement Reinforcement [in. (cm)]	
		WWR	Cap Bar[1]
7-NU1100-I	NDOR BOPP[2]	D4@4 (10) entire length	No. 3@12 (31) entire length
7-NU1100-II	AASHTO[3]	D11@6 (15) for 72 (183) E.E.	No. 3@6 (15) for 72 (183) E.E.
7-NU1100-III	AASHTO+NDOR	D11@6 (15) for 72 (183) E.E., D4@4 (10) middle	No. 3@6 (15) for 72 (183) E.E., No. 3@12 (31) middle

[1] Cap bar is shown in Figure 3.5
[2] 2008 Nebraska Department of Roads Bridge Operations, Policy, and Procedure
[3] 4th Ed. AASHTO LRFD

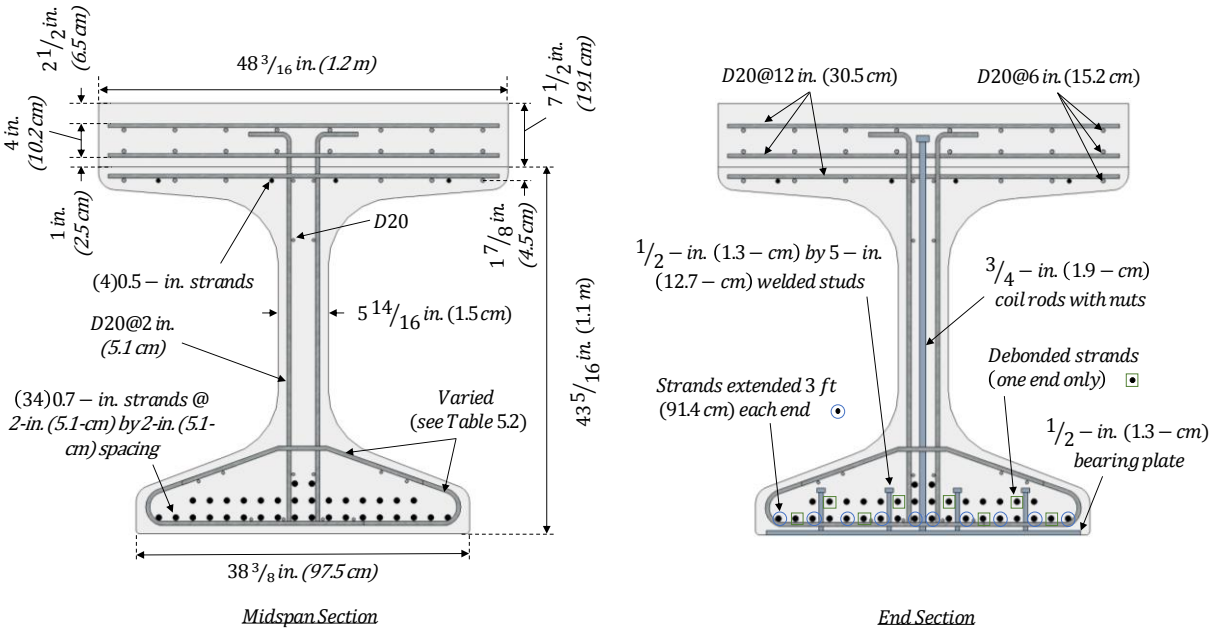

Figure 3.4: Cross-section and reinforcement details for NU1100 girders

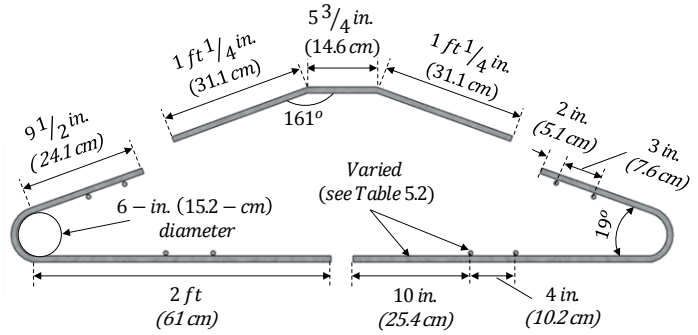

Figure 3.5: Confinement reinforcement for NU1100 girders (top piece is the cap bar)

Strand slip was monitored to identify bond failure (reported by the respective authors as bond slip greater than 0.01 in. or 0.25 mm) if it preceded strand development and nominal capacity. Next, the opposite span of the specimen was tested in a shear-critical loading configuration with an a/d_p ratio of 1.9. To correctly model the shear test, it was necessary to capture the stiffness reduction caused by the damage incurred during the

development length test; hence, in this case, both tests were modeled. Strand slip was monitored experimentally also at the shear test span.

A number of critical member and testing details were not provided in the report which necessitated several assumptions in the analyses. Tadros & Morcous (2011) did not distinguish between the live and dead ends in the descriptions of the test spans (each end had slightly different conditions). The end of the specimen that was tested in shear consisted of a total of eight debonded strands: a group of four in the middle row for a length of 7 ft (2 m) and a group of four in the bottom row for a length of 3.5 ft (1 m) which is the transfer length of a 0.7-in. (17.8-mm) diameter strand (AASHTO, 2014). In addition, ten of the strands at this end were extended, bent and embedded into an end diaphragm which is common practice in the state of Nebraska. Note that ten strands were extended 3 ft (91.4 cm) at each end, but only the debonded-end consisted of an end diaphragm for anchorage. Also, note that the debonded-portions of these strands were not included in the models, and that these strands were permitted to slip at both ends. Strands that were embedded in the end diaphragm were restrained from slipping, to represent the effect of the diaphragm anchorage.

Figure 3.6 illustrates the modeling approach used for the strands comprising the NU-Girders.

The dimensions of the loading plates were not provided, and there were discrepancies between details given regarding the number of loading points used in the tests. The load plate was assumed to be 1-in. (2.5-cm) thick, 12-in. (31-cm) wide in the girder's longitudinal direction, and 24-in. (61-cm) in length across the width of the specimen.

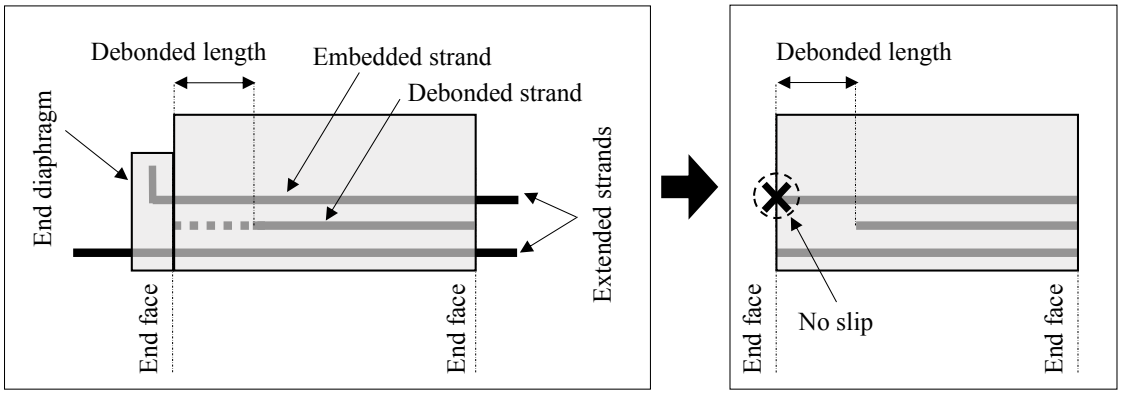

Figure 3.6: Modeling of strand boundaries (elevation view): (a) as-built condition (b) modeling approach

As noted previously, only nominal concrete and reinforcement material properties were reported. The strand material properties were provided in terms of measured properties from two different strand manufacturers. It was not clear which group of strands was used in the fabrication of the NU1100 girders. Therefore, an average of the two groups was used for modeling purposes.

The NU-Girders were fabricated with embedded bearing plates that were 0.5-in. (12.7-mm)-by-18-in.-by-36-in. (1.3-cm-by-46-cm-by-91-cm) in dimension with eight ½-in.-diameter-by-5-in.-long (1.3-cm-by-13-cm) steel studs that were welded to the bearing-plate and embedded in the concrete. Additionally, the girders contained four ¾-in.-diameter-by-46-in.-long (2-cm-by-117 cm) threaded rods at the center of the web that were welded to the bearing-plates at each end (see Figure 3.4). Both threaded rods and steel studs were modeled with perfect bond as they were welded to the bearing plates. However, it should be noted that the bearing plates were not included in the ATENA model. The assumptions described herein, particularly those pertaining to material properties and load-plate dimensions, are likely sources of errors in the analyses performed. Table 3.3

summarizes the design and test setup used for the NU-Girders. “B” refers to the bonded end and “De-B” refers to the debonded end.

Table 3.3: Specimen and test setup details of NU-Girders with 0.7-in. (17.8-mm) diameter strand

		Specimen	7-NU1100-I		7-NU1100-II		7-NU1100-III	
		End	B	De-B	B	De-B	B	De-B
Test Setup		Beam Length [ft (m)]	40 (12.2)					
		Span Length [ft (m)]	39 (11.9)	24 (7.3)	39 (11.9)	24 (7.3)	39 (11.9)	24 (7.3)
		Test Span Length [ft (m)]	13.5 (4.1)	7.5 (2.3)	13.5 (4.1)	7.5 (2.3)	13.5 (4.1)	7.5 (2.3)
		a/d_p	3.4	1.9	3.4	1.9	3.4	1.9
Transverse Reinforcement		Stirrup Type	WWR					
		Stirrup Spacing (2)D20 [in. (cm)]	2 (5.1)					
		Nominal F_y [ksi (MPa)]	75 (517)					
Concrete		Specified Girder f'_{ci} [ksi (MPa)]	7.8 (53.8) (Patzlaff, Morcous, Hanna, & Tadros, 2012)					
		Specified Girder f'_c [ksi (MPa)]	10 (69)					
		Specified Deck f'_c [ksi (MPa)]	8 (55)					
		Deck Dimensions (width-by-thickness)	48.2-in.-by-7.5-in. (122.4-cm-by-19.1-cm)					
Strands		F_y	247 ksi (1,700 MPa)					
		F_u	277 ksi (1,909 MPa)					
	Bottom	A_{ps}	10 in^2 (64.5 cm^2)					
		f_{pi}	202.5 ksi (1,396 MPa)					
		e_{ps}	16.6 in. (42.2 cm)					
	Top	A_{ps}	0.6 in.^{2} (4 cm^2)					
		f_{pi}	202.5 ksi (1,396 MPa)					
		e_{ps}	22.2 in. (56.4 cm)					

3.3 RESULTS AND DISCUSSION

This section provides an overview of the results from the numerical validation studies done for release, development length and shear tests. The section is divided into two major sub-sections discussing prestress transfer and load-deflection behavior.

3.3.1 Prestress Transfer

The release of prestressed girders is achieved by detaching the strands from the jacking equipment (e.g., cutting strands, retracting the loading rams, etc.) and thus, facilitating the transfer of the prestressing force to the concrete by way of bond between the strands and concrete. In the 6-Tx-Girders series, the top strands were first cut then the bottom strands were gradually released using hydraulic rams (O'Callaghan, 2007). The applied prestress force is limited by the maximum allowable tensile and compressive stresses that subsequently develop in the end region. The 2015 TxDOT AASHTO LRFD Bridge Design Guidelines, permits compressive and tensile stresses up to $0.65 \cdot f'_{ci}$ (ksi) and $0.24 \cdot \sqrt{f'_{ci}}$ (ksi), respectively, at the time of release.

Following release, the strand force is zero at the girder end and gradually increases to the applied prestressing force at the transfer length, L_t. As a result of the transfer of these forces, the girder develops camber and shortens elastically. Prestress transfer typically results in cracks in the end-region caused by spalling, bursting or splitting stresses. The procedure used to model the release test in ATENA is described in Section 2.2.1.

Release test measurements were provided for the Tx-Girders, only. Table 3.4 lists a comparative summary of the computed and experimental results from the release tests and Figure 3.7 demonstrates the comparison in release damage. The ATENA calculations are reported for the time immediately following release. However, because of the

sensitivity of the FEA results to modeling inputs and assumptions, it is arguably more meaningful to assess adequacy on the basis of damage distribution rather than maximum crack widths. The transfer length reported in Table 3.4 is not calculated based on the 95 % AMS method (Russell & Burns, 1993), rather by observation of a plateau in the strand strain gage data.

Table 3.4: Release test results for Tx-Girders with 0.6-in. (15.2-mm) strands

Girder	6-Tx28-I		6-Tx28-II		6-Tx46-I	
Results	Measured	ATENA	Measured	ATENA	Measured	ATENA
w_{crack} max. [in. (mm)]	0.005 (0.127)	0.005 (0.131)	0.009 (0.230)	0.005 (0.110)	0.007 (0.178)	0.007 (0.165)
L_t[1] [in. (cm)]	36 (91)	20 (51)	36 (91)	32 (81)	36 (91)	30 (76)
$\sigma_{s,max}$ [ksi (MPa)]	22 (151)	21 (142)	32 (221)	16 (113)	22 (151)	24 (162)

[1] Strands were monitored up to a length of 42 in. (107 cm) compared to the 36-in. (91-cm) theoretical estimation of transfer length for 0.6-in. (15.2-mm) strands (AASHTO, 2014).

Discrepancies between the measured and predicted transfer lengths may have resulted from inaccurate bond modeling and/or concrete properties. Another factor that may have contributed to the discrepancies is that it was not certain whether measurements were recorded immediately following prestress release, or some other time. Based on tests conducted on Tx-Girders with 0.7-in. (17.8-mm) diameter strands (the present study), crack widths developed at prestress transfer may continue to grow for several days after release. Further, the perfect bond assumption applied to all non-prestressing reinforcement may also have contributed to discrepancies associated with the computed reinforcement stresses. Numerical results showed that the reinforcing bars tied to the R-Bar stirrups developed up to 32 ksi (221 MPa) which approximately matched the experimentally

measured stress in the R-Bars according to strain gage data. Note that this level of stress exceeds the AASHTO-recommended end-region stress limit of 20 ksi (138 MPa) (AASHTO, 2014).

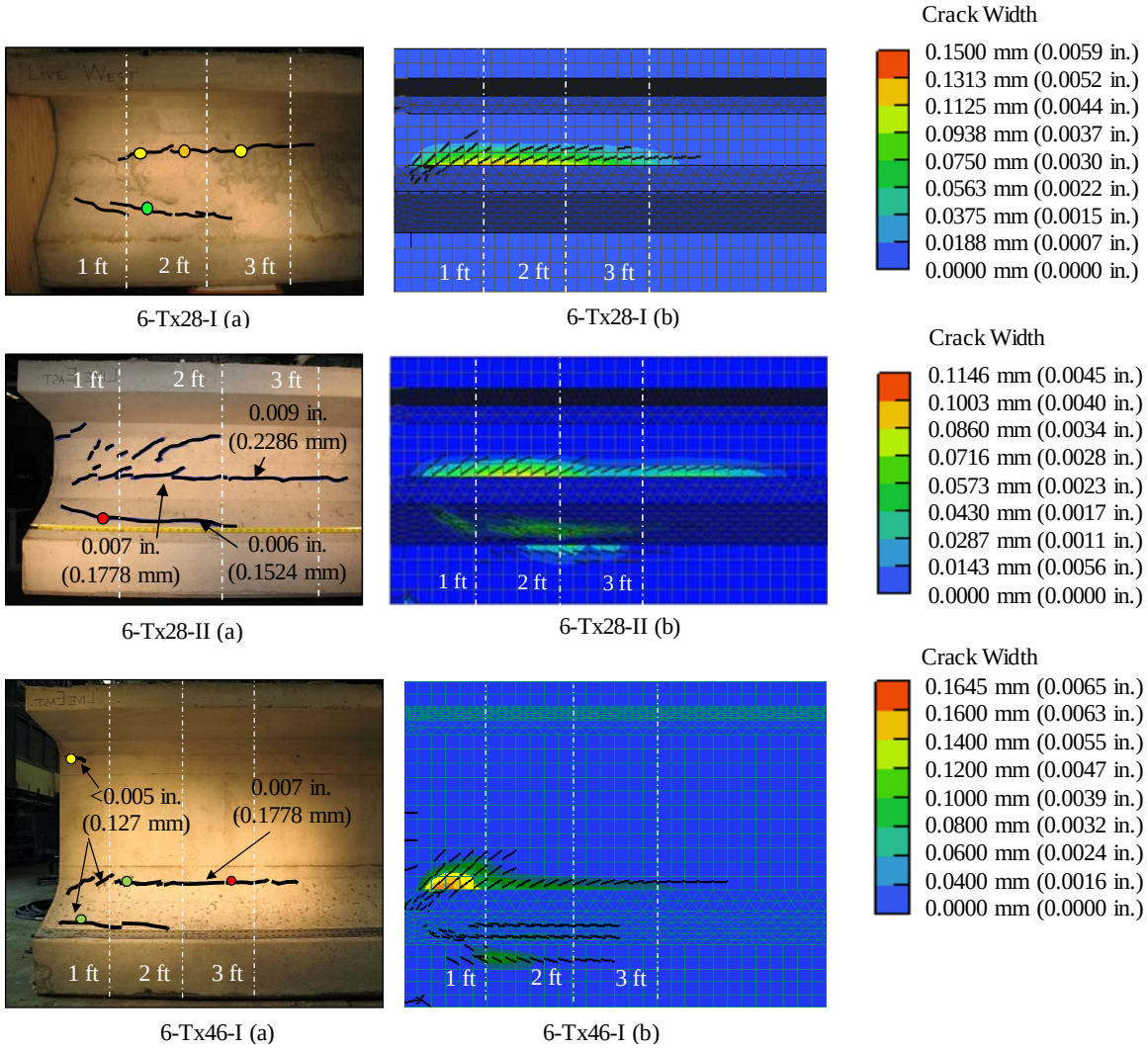

Figure 3.7: Live end release cracks of Tx-Girders with 0.6-in. (15.2-mm) strands (elevation view): (a) measured (b) ATENA

The primary difference in the design of 6-Tx28-I and 6-Tx28-II is that 6-Tx28-I was released at a concrete compressive strength of 10 ksi (69 MPa) whereas 6-Tx28-II was

released at a strength of 6.5 ksi (45 MPa). 6-Tx28-II exhibited more concrete damage and developed larger steel stresses as a result of the lower strength concrete. Minimal spalling cracks were also observed in the web of 6-Tx28-II. Figure 3.8 illustrates the variation of strand force along those strands that were monitored during the release experiments. Given the level of scatter in the experimental data, the analytical results provide a reasonable agreement with experiment data. ATENA captured the aspects of end-region serviceability that are of interest to the present study: stirrup stresses, concrete damage and transfer length.

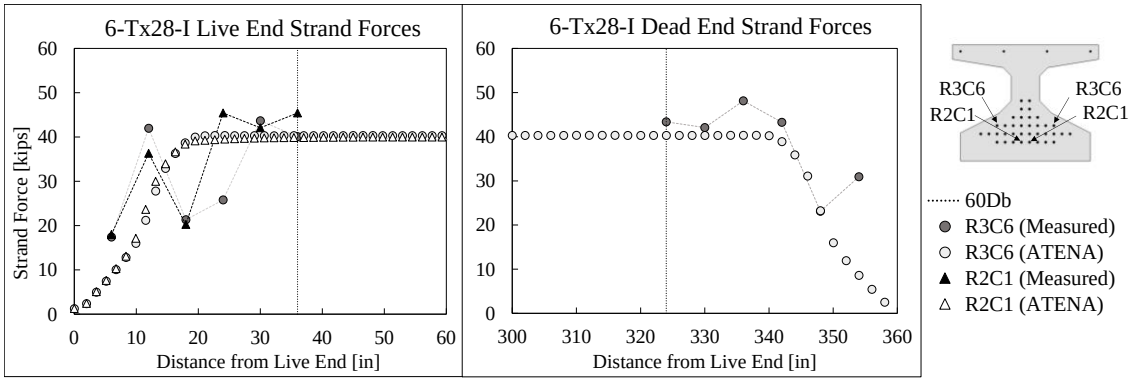

Force (kips) · 4.45 = force (kN); distance (in.) · 2.54 = distance (cm).

Figure 3.8: Comparison of ATENA and measured strand forces after release

3.3.2 Load-Deflection Behavior

This section summarizes the results from the analyses of the development length and shear tests of the six specimens in terms of failure modes and load-deflection behavior. As noted previously, the elastic stiffness and cracking load of all tests were in good agreement with the observed stiffness; however, the ultimate capacities were underestimated. Figure 3.9 demonstrates the measured and predicted load-deflection

behaviors of the Tx-Girders and Figure 3.10 compares predicted and measured shear capacities. Tensile yielding was estimated to occur in the stirrups at the location of maximum concrete damage. The stirrups under the load-plate showed signs of compression yielding. Actual reinforcement strains were not measured during the experiments and, as such, could not be used for comparison.

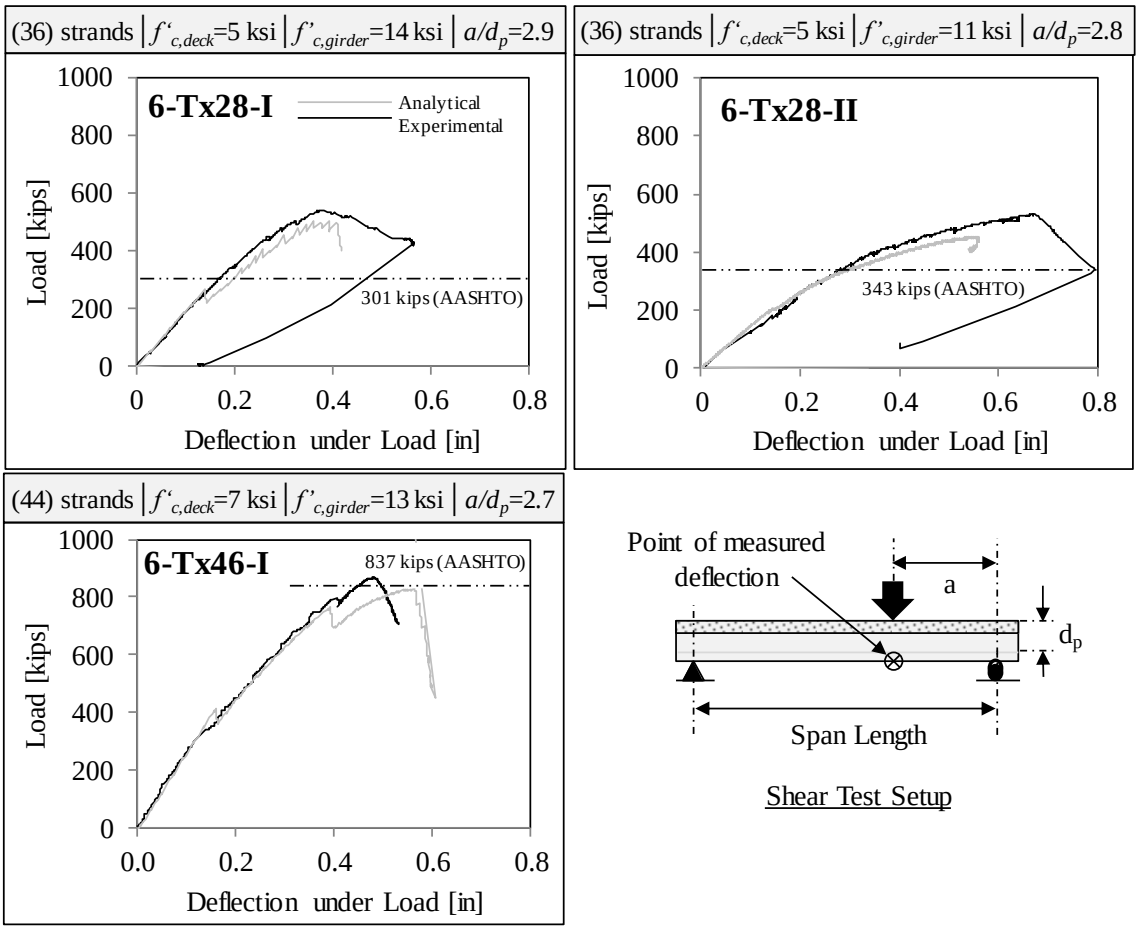

Force (kips) · 4.45 = force (kN); deflection (in.) · 2.54 = distance (cm).

Figure 3.9: Shear tests of Avendaño Tx-Girders with 0.6-in. (15.2-mm) strands

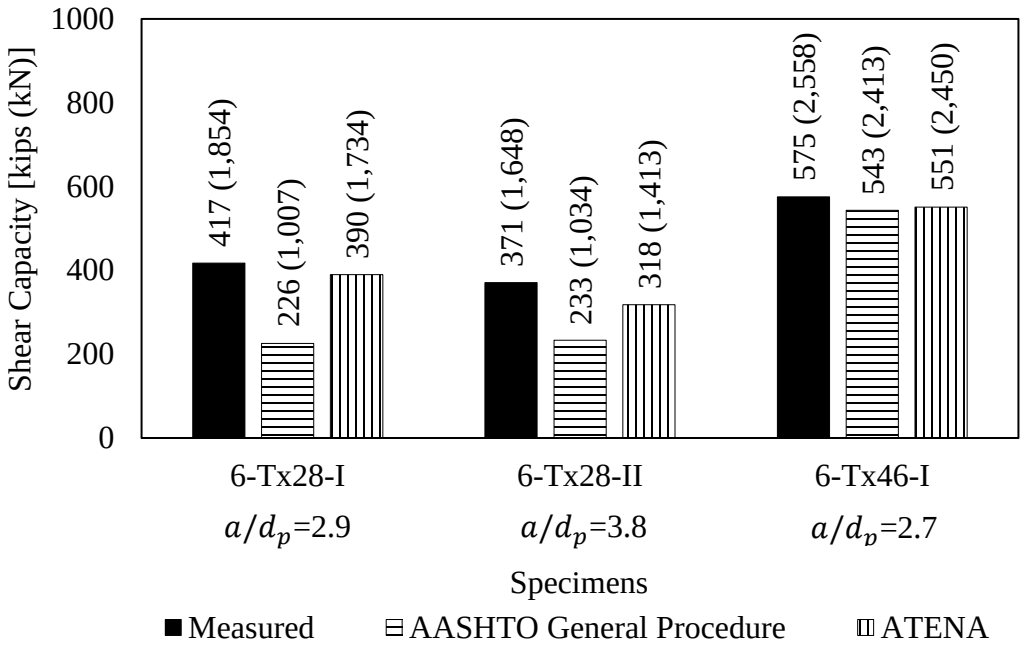

Force (kips) · 4.45 = force (kN);

Figure 3.10: Comparison of calculated and measured shear capacities

Likely as a result of the large number of assumptions required in developing the FEA models, greater levels of error were obtained in the numerical results for the NU-Girders than the Tx-Girders. Models of the development length tests of the NU-Girders exhibited premature shear failures prior to developing the experimentally measured capacities.

Based on a photo (Figure 3.11) showing one NU1100 specimen after the first experiment, visibly long diagonal web cracks had formed prior to the shear test. Further, the shear capacity of the specimen in the development length test was calculated to be 702 kips (3,123 kN) (AASHTO LRFD General Procedure 5.8.3.3). The maximum applied load during the development length test was not indicated, but observed from the reported load-deflection plots to be approximately 1,075 kips (4,782 kN) and the shear developed in the

specimen under such applied load at the tested a/d_p ratio of 3.4 is 703 kips (3,127 kN) in addition to the shear induced by self-weight of the specimen and loading frame. As a result, the specimen was loaded slightly above its shear capacity. Even though the load resisting response of the specimen did not exhibit a significant drop during the experiment, the finite element model of the specimen demonstrated shear failure which may be justifiable given the AASHTO-calculated shear capacity. It should also be noted that this degree of computed versus experimentally measured strength discrepancy is to be expected as ATENA had also underestimated the shear capacity in the Tx-Girders with 0.6-in. (15.2-mm) strands. Lastly, it is important to note that the actual specimen also demonstrated visible and web-shear damage (Figure 3.11).

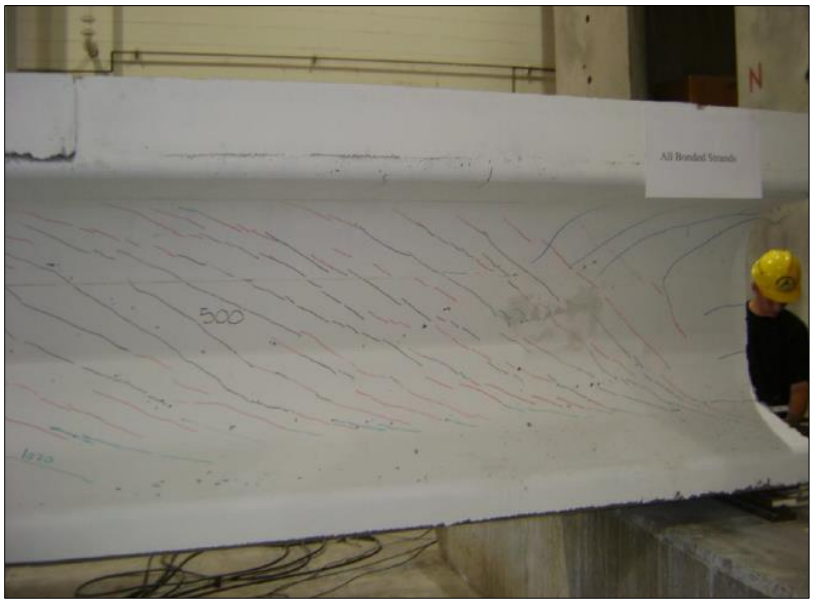

Figure 3.11: Visible damage after the development length test in one NU1100 girder (Tadros & Morcous, 2011)

As a result of the numerical shear failure, the specimen could not be numerically unloaded in a manner that would represent the damage in the actual specimen. The level of damage developed during the experiment was not explicitly reported; however, Figure 3.11 provides a visual reference. Attempts in capturing the damaged beam's stiffness during the second "shear test" were not beneficial and these tests are not described further in this report. The important takeaway is that ATENA captured the stiffness of the load-deflection response during the development length tests and conservatively predicted the shear capacity.

Prior to this observation, it was suspected that relatively large bond slip may have prevented the model from developing its full flexural capacity. Force (kips) · 4.45 = force (kN); displacement (in.) · 2.54 = displacement (cm).

Figure 3.12 demonstrates the sensitivity of the development length test prediction to bond slip by comparing a model with perfect bond against the typical Bigaj (1999) bond assumption. The perfect bond is illustrated for comparison, only. It was observed that the bond slip with the Bigaj (1999) bond model was arguably reasonable.

Tadros & Morcous (2011) reported strand slips that were measured using potentiometers installed at the ends of the extended strands located at the tested end. It is important to note that during the development length test, girder 7-NU1100-III, containing the greatest amount of confining reinforcement was reported to have the largest strand slip. Tadros & Morcous (2011) suggested that this was caused by the smaller 3-in. wide (76-mm) bearing-plate which induced high stress concentrations in the bottom flange during loading and led to large slippage at the girder end. This issue was addressed for the two specimens which were tested following 7-NU1100-III. The bearings used for the other two

specimens were 12-in.-by-30-in. (30.5-cm-by-76.2-cm). Table 3.5 lists the measured and predicted maximum slip at nominal capacity for each specimen.

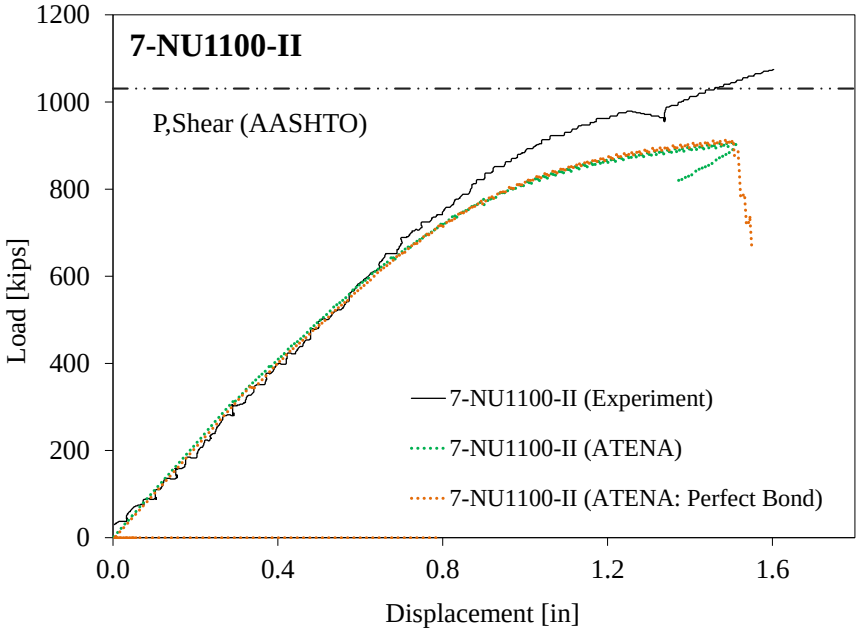

Force (kips) · 4.45 = force (kN); displacement (in.) · 2.54 = displacement (cm).

Figure 3.12: Effect of bond in 7-NU-1100-II development length test

Table 3.5: Strand slip measured at nominal capacity of NU-Girders

Test	Specimen	7-NU1100-I		7-NU1100-II		7-NU1100-III	
	Result	Meas.	ATENA	Meas.	ATENA	Meas.	ATENA
Dev. Length	Slip [in. (mm)]	0.018 (0.457)	0.015 (0.381)	0.007 (0.178)	0.015 (0.381)	0.040 (1.016)	0.015 (0.381)

Figure 3.13 provides a comparison of the predicted and measured load-deflection plots using the Bigaj (1999) bond model. The numerically estimated capacity of the NU-

Girders was approximately 890 kips (3,959 kN); 14 % less than the AASHTO capacity of 1031 kips (4,586 kN).

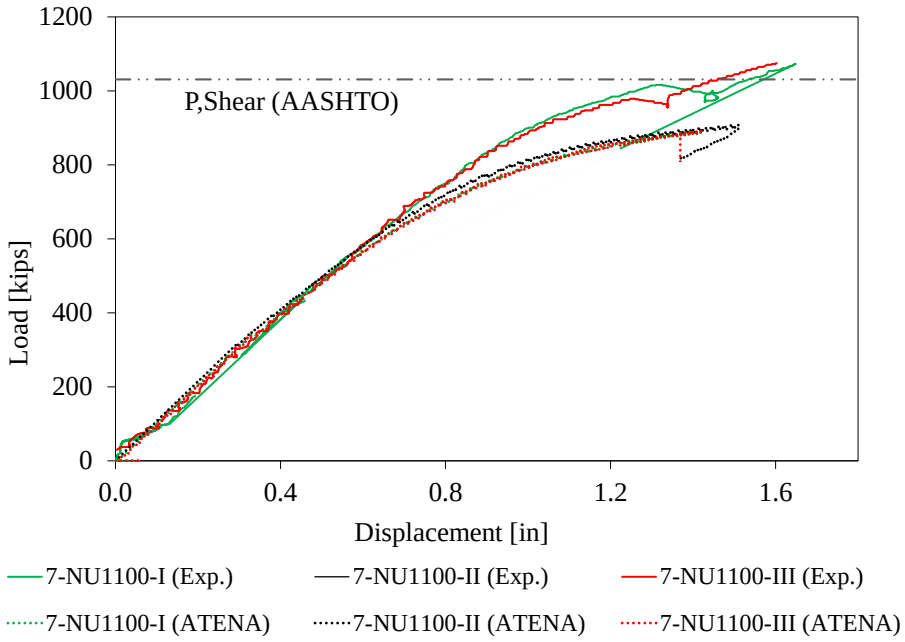

Force (kips) · 4.45 = force (kN); displacement (in.) · 2.54 = displacement (cm).

Figure 3.13: Development length tests of NU-Girders with 0.7-in. (17.8-mm) diameter strands

3.3.3 Crack Patterns and Failure Modes

An important measure of the adequacy of the FEA was the correct prediction of the failure mode. The Tx-Girders experienced horizontal shear failure at the interface between the bottom flange and web characterized with horizontal cracks and relative displacement along this interface. The Tx-Girders were instrumented with strain gages for the release tests; however, no measurements were recorded during the shear tests. Figure 3.14 through

Figure 3.16 provide visual comparisons of the damage just after peak load in the 6-Tx-Girders.

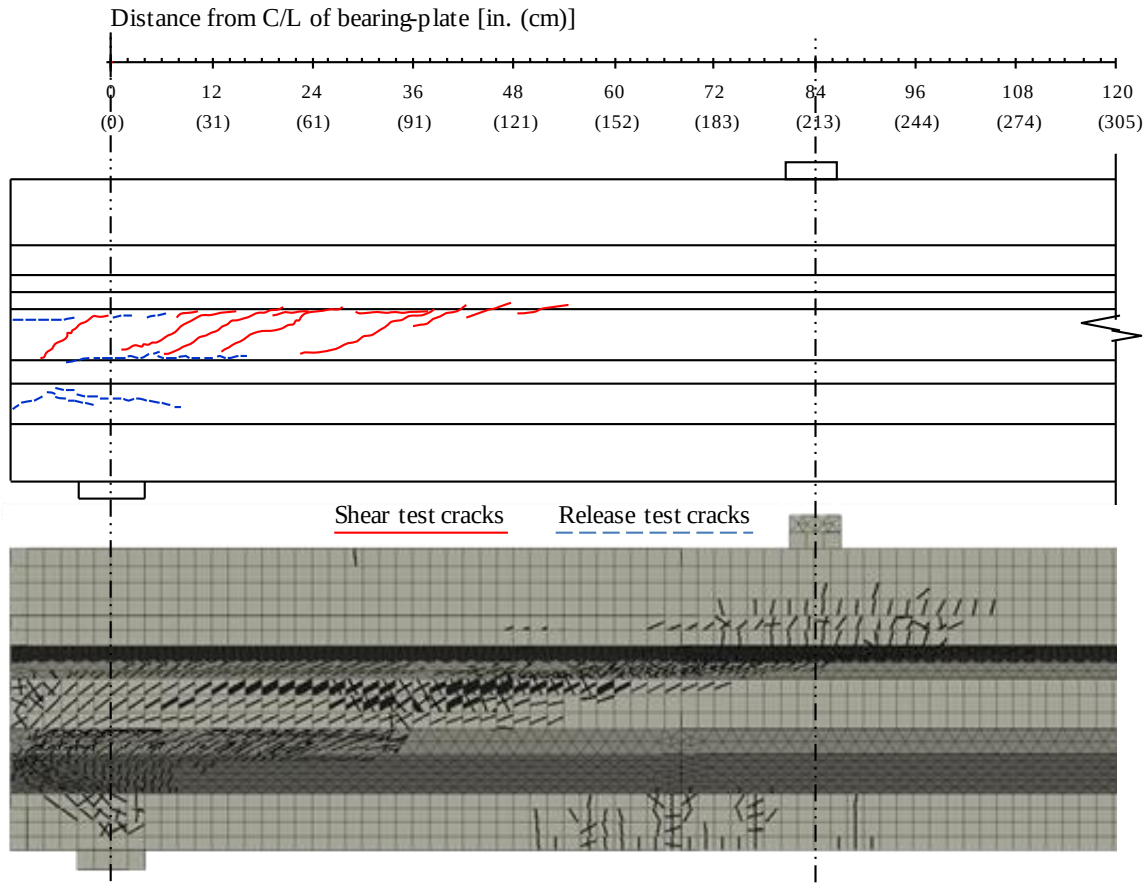

Figure 3.14: Shear test damage in 6-Tx28-I: (a) experiment (adapted from Avendaño (2008)), (b) ATENA

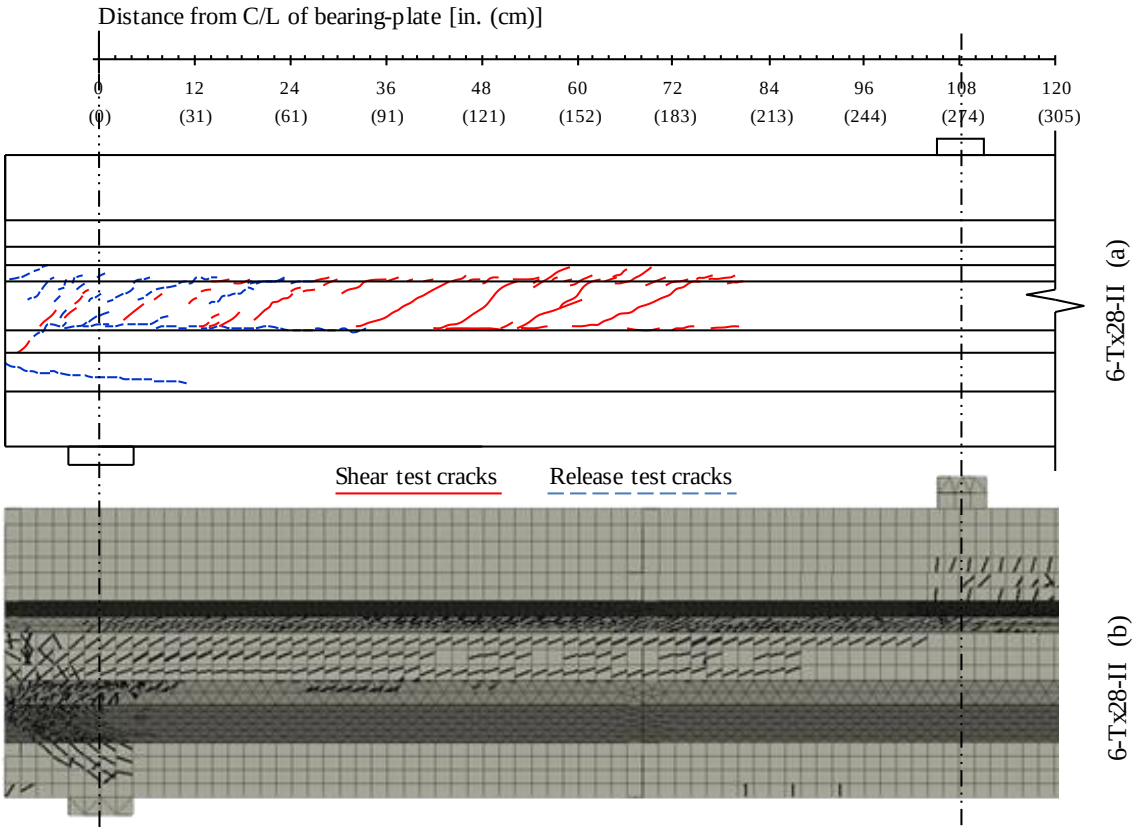

Figure 3.15: Shear test damage in 6-Tx28-II: (a) experiment (adapted from Avendaño (2008)), (b) ATENA

All the specimens formed distinct horizontal cracks at the interface between the web and top or bottom flange. This form of horizontal cracking was also captured in the analyses.

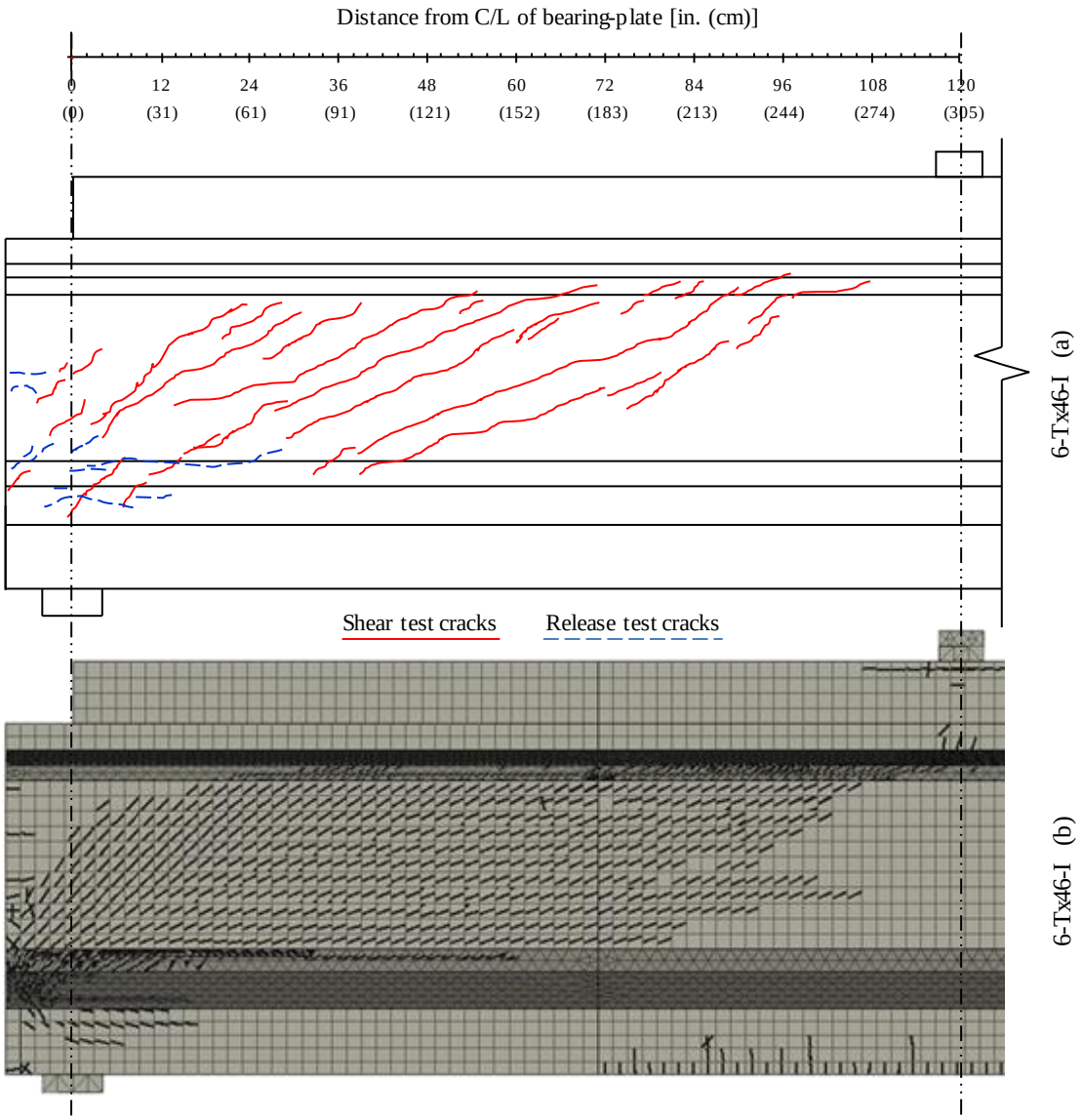

Figure 3.16: Shear test damage in 6-Tx46-I: (a) experiment (adapted from Hovell et al. (2012) and O'Callaghan (2007)), (b) ATENA

3.4 Application to Tx-Girders with 0.7-in. Strands

Following the verification of experiments found in the literature, the specimens fabricated for the present study were also modeled using ATENA. Two 46-in. (1.17-m)

deep and two 70-in. (1.78-m) deep girders were fabricated at FSEL containing 0.7-in. (17.8-mm) diameter strands. The focus of the study was end-region serviceability and shear behavior of I-Girders with 0.7-in. (17.8-mm) diameter strands. The design objectives for the first two Tx46 girders were to maximize eccentricity and strand forces and therefore increase spalling and bursting stresses in the end-region, respectively. The next two (Tx70) girders were fabricated with the objective of maximizing eccentricity using the deepest Tx-Girder currently available. 7-Tx70-I had the largest eccentricity among all other specimens considered in the verification study. 7-Tx70-II was released at a compressive strength of 8 ksi (55.2 MPa) to assess potential benefits associated with permitting higher compressive release strengths.

The specimens were tested under shear-critical loading conditions. The first two Tx46 girders were tested under four-point loading as shown in Figure 3.17 (a), with an a/d_p ratio of 3.0. Table 5.6 lists the specimen and test setup details of the Tx-Girders with 0.7-in. (17.8-mm) diameter strands.

Since the experiments were conducted in collaboration with this numerical study, necessary details were available for accurate numerical estimation. Unlike the other specimens discussed in this document, the Tx-Girders with 0.7-in. (17.8-mm) diameter strands contained vibrating wire gages (VWG) which were used to record the prestress loss history of the specimen up to the time of load testing. The measured change in strain at the midspan at the centroid of the specimens was on average -0.35×10^{-3}in./in. as recorded after release up to the time of load test. To incorporate the measured prestress losses into the models, the standard shrinkage magnitude of -0.2×10^{-3}in./in. introduced in Section 2.2.2 was replaced by -0.35×10^{-3}in./in. for Tx-Girders with 0.7-in. (17.8-mm) diameter strands. This shrinkage was applied through ten analysis steps (rather than one)

for numerical stability. The former value did however yield a good comparison between the analytical and experimental results of the Tx-Girders with 0.6-in. (15.2-mm) strands and the NU-Girders.

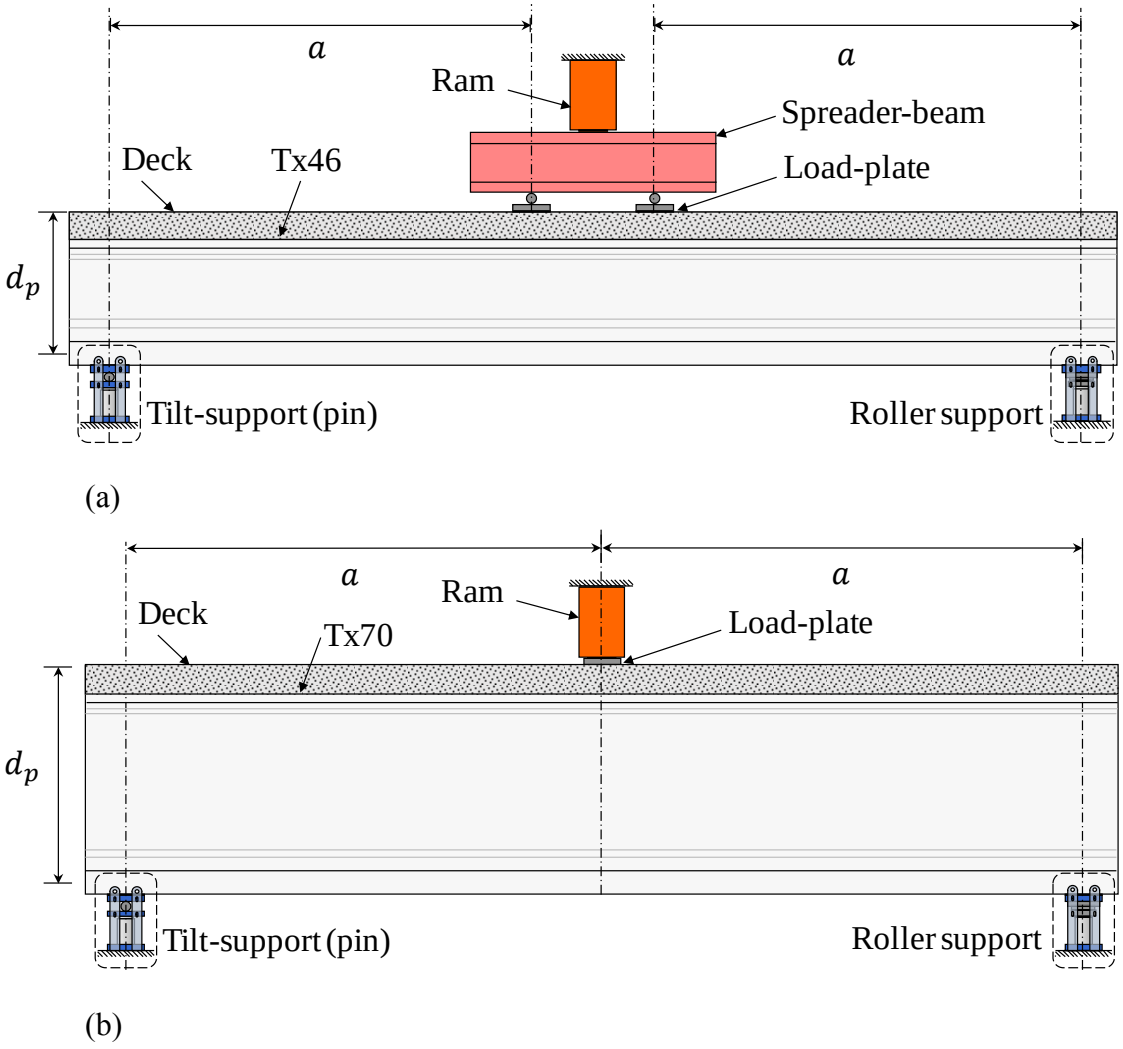

Figure 3.17: Shear test setup of Tx-Girders with 0.7-in. (17.8-mm) diameter strands (elevation view): (a) 7-Tx46-I and 7-Tx46-II, (b) 7-Tx70-I and 7-Tx70-II

Overall, the predicted crack patterns at release matched the observed crack patterns with high accuracy. The shear capacities were underestimated, as was typically the case in the validations studies, and the elastic stiffness was generally predicted well for all specimens. Table 5.6 summarizes the specimen and test setup details.

Table 3.6: Specimen and test setup details of Tx-Girders with 0.7-in. (17.8-mm) diameter strands

	Specimen		7-Tx46-I	7-Tx46-II	7-Tx70-I	7-Tx70-II
Test Setup	Beam Length		30 ft (9.1 m)			
	Span Length		28.5 ft (8.7 m)			
	Shear Span Length ft (m)		12.7 (3.9)	10.9 (3.3)	14.3 (4.3)	14.3 (4.3)
	a/d_p		3.0		2.3	
Transverse Reinforcement	Stirrup Type		Standard			
	Stirrup Spacing (2)No. 4 [in. (cm)]		1@2.5 (6.4) E.E., 12@3 (7.6) E.E., r@6 (15.2)		1@2.5 (6.4) E.E., 12@3 (7.6) E.E., r@8 (20.3)	
	Measured F_y [ksi (MPa)]		61 (421)		72 (498)	
	Extra (2)No. 6 [in. (cm)]		1@1.9 (4.8) E.E., 12@3 (7.6) E.E.			
	Measured F_y [ksi (MPa)]		72 (495)		70 (483)	
Concrete	Girder f'_{ci} [ksi (MPa)]		5.8 (40)	5.2 (36)	6.5 (45)	8.3 (57)
	Girder f'_c [ksi (MPa)]		7.6 (52)	6.9 (48)	10.7 (74)	12.7 (88)
	Deck f'_c [ksi (MPa)]		10.7 (74)	7.9 (55)	7.9 (55)	9.2 (63)
	Deck Dimensions (width-by-thickness)		34-in.-by-8-in. (86.4-cm-by-20.3-cm)		40-in.-by-8-in. (101.6-cm-by-20.3-cm)	
Strands	Meas. F_y [ksi (MPa)]		232 (1,600)			
	Meas. F_u [ksi (MPa)]		276 (1,903)			
	Bottom	A_{ps} [in.^{2} (cm^2)]	7.1 (45.5)	8.8 (56.9)	8.2 (53.1)	12.4 (79.7)
		f_{pi} [ksi (MPa)]	202.5 (1,396)			
		e_{ps} [in. (cm)]	16.8 (42.7)	9.7 (24.6)	28.4 (72.2)	27.4 (69.6)
	Top	A_{ps} [in.^{2} (cm^2)]	1.2 (7.6)			
		f_{pi} [ksi (MPa)]	157.5 (1,086)	202.5 (1,396)	110 (758)	202.5 (1,396)
		e_{ps} [in. (cm)]	23.9 (60.7)		36.1 (91.7)	

3.4.1 Prestress Transfer

The following figures present crack distributions in the end-regions of the Tx-Girders. The prestressing forces were released by gradually retracting the hydraulic rams of both the top and bottom strands maintaining a consistent ratio of top and bottom strand forces. As strand eccentricity in 7-Tx46-I was greater than in 7-Tx46-II, the eccentricity-induced spalling cracks in the web of 7-Tx46-I can be distinguished from the more prominent bursting cracks parallel to the strands in the bottom flange of 7-Tx46-II.

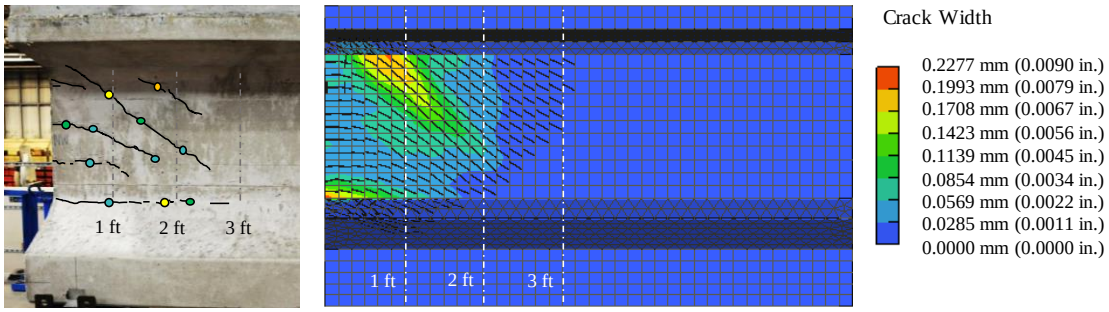

(a) (b)

Figure 3.18: 7-Tx46-I release cracks (live end): (a) measured (b) ATENA prediction

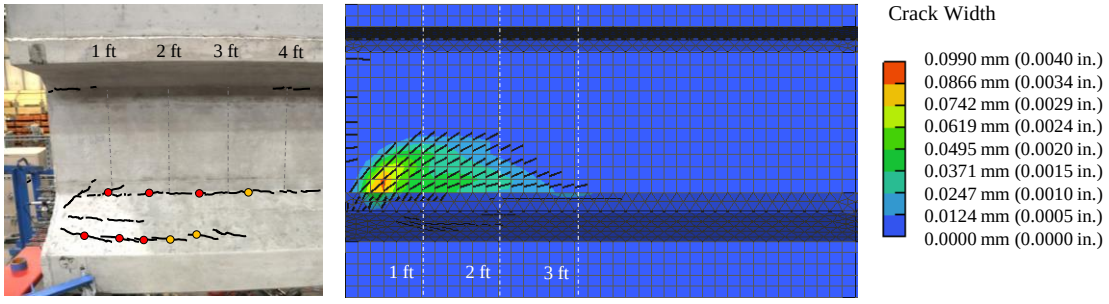

(a) (b)

Figure 3.19: 7-Tx46-II release cracks (live end): (a) measured (b) ATENA prediction

7-Tx70-I had the largest prestressing force eccentricity in the 7-Tx-Girder group of specimens. Eccentricity-induced spalling cracks in the web reached 0.008 in. (0.2 mm) in width. Essentially no bursting cracks were visible. A similar pattern with smaller crack widths was observed in 7-Tx70-II which had a higher compressive strength.

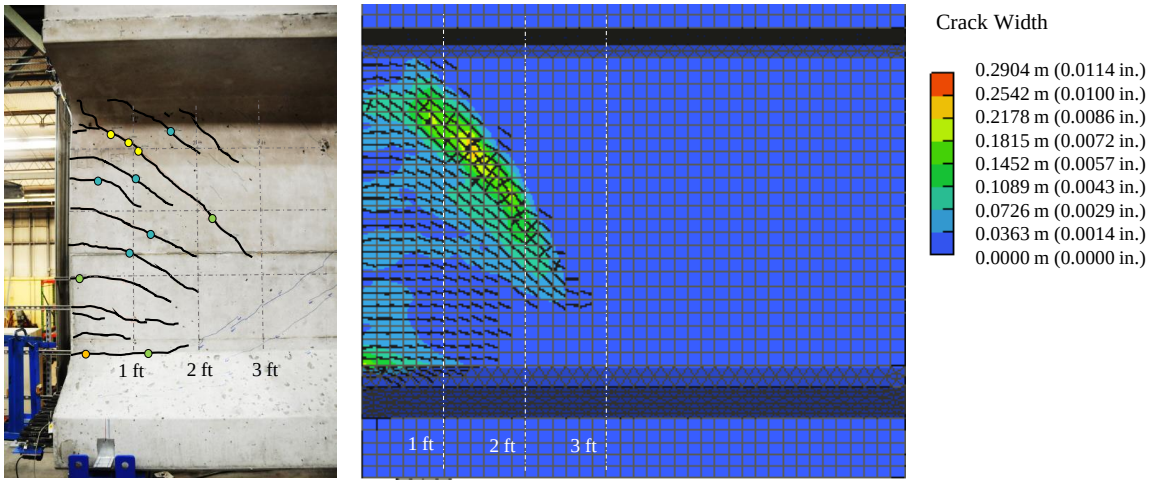

(a) (b)

Figure 3.20: 7-Tx70-I release cracks (live end): (a) measured (b) ATENA prediction

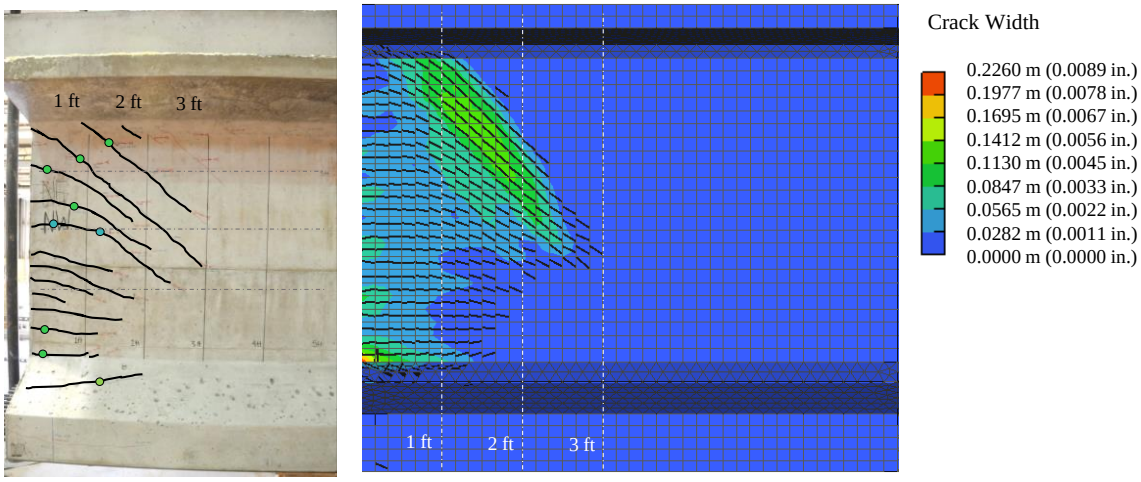

(a) (b)

Figure 3.21: 7-Tx70-II release cracks (live end): (a) measured (b) ATENA prediction

The following table summarizes the measured response parameters of the release tests for the Tx-Girders with 0.7-in. (17.8-mm) diameter strands. All measurements correspond to the time immediately following prestress transfer. Crack width comparisons are conducted for the live ends only. The transfer lengths reported in the following table are calculated based on the 95 % AMS method.

Table 3.7: Release test results for Tx-Girders with 0.7-in. (17.8-mm) diameter strands

Results	7-Tx46-I		7-Tx46-II		7-Tx70-I		7-Tx70-II	
Girder	Meas.[1]	ATENA	Meas.	ATENA	Meas.	ATENA	Meas.	ATENA
w_{crack} max. [in. (mm)]	0.008 (0.2)	0.009 (0.23)	0.004 (0.1)	0.004 (0.1)	0.006 (0.15)	0.007 (0.18)	0.007 (0.18)	0.008 (0.2)
L_t[2] [in. (cm)]	40-41 (102-104)	32 (81)	28-31 (71-79)	32 (81)	30-41 (76-104)	32 (81)	34-42 (86-107)	32 (81)
$\sigma_{s,max}$[3] [ksi (MPa)]	19 (131)	22 (153)	14 (97)	9 (64)	25 (172)	25 (175)	26 (179)	32 (218)

[1] Measured
[2] The maximum bottom strand transfer length from either the dead or the live end. Four strands were monitored at each end and the measured transfer lengths varied from 28-42 in. (71-107 cm).
[3] The measured stirrup strains were converted to stresses assuming a modulus of 29,000 ksi (199,948 MPa).

A brief comparison of transfer length in the Tx-Girders with 0.7-in. (17.8-mm) diameter strands as opposed to Tx-Girders with 0.6-in. (15.2-mm) strands, shows that the transfer length of 0.7-in. (17.8-mm) diameter strands is larger. It must be noted that strain measurements reported by O'Callaghan (2007) for 0.6-in. (15.2-mm) strands were recorded up to a length of 42 in. (107 cm) into the beam. The decision that transfer length had been identified was based on locating the expected strand stress along the strand. Strand stresses were estimated from strain gage measurements and an assumed strand modulus of elasticity. This determination may be subject to errors because of the

uncertainty in expected strand stresses and the modulus of strand steel. In contrast with the observed transfer length variation with strand diameter in Tx-Girders, Tadros & Morcous (2011) found the transfer length of 0.7-in. (17.8-mm) diameter strands to be approximately 26 in. (66 cm) in a different series of tests on NU900 girders. The reported transfer lengths of NU-Girders were estimated using the 95 % Average Maximum Strain (AMS) method (Russell & Burns, 1993) and strains were measured by DEMEC gage readings on the concrete surface before and after release. However, the NU900 transfer length measurements do not represent an equivalent comparison since the NU900 girders were fabricated with UHPC concrete with a release strength of approximately 12 ksi (83 MPa) which, relative to 6 ksi (41 MPa) concrete, would be expected to enhance bond and reduce the transfer length. For comparison purposes, the recommended transfer length for 0.7-in. (17.8-mm) diameter strands is 42 in. (107 cm) based on AASHTO LRFD (2014) and ACI 318 (2014) ($60 \cdot D_b$). The measured transfer length of Tx-Girders varied from 28 to 42 in. (71 to 107 cm).

3.4.2 Shear Behavior

Many factors may contribute to the response of a prestressed concrete specimen under shear-critical loading. Force (kips) · 4.45 = force (kN); deflection (in.) · 2.54 = deflection (cm).

Figure 3.22 illustrates the ATENA predictions (dotted lines) of the shear tests on the Tx-Girders with 0.7-in. (17.8-mm) diameter strands, as compared with the experiments (solid lines). Table 3.8 lists the predicted and measured capacities. In general, the initial stiffness of the calculated load-displacement plots match the measured stiffness.

Observed yielding of the stirrups was captured in all models except for in 7-Tx46-II for which yielding occurred just at the onset of the ultimate capacity of the specimen. Strain development in the No. 4 stirrups were monitored over a distance of 62.5 in. (1.6 m)

into the beams which was compared with the computed stirrup yielding in ATENA. Table 3.8 lists the predicted and measured capacities (excluding specimen and frame weight). The AASHTO calculated capacities are based on the minimum predicted by the General Procedure (5.8.3.3) and Anchorage Provisions (5.8.3.5). Specimens 7-Tx46-I and 7-Tx70-I were governed by AASHTO 5.8.3.5 Anchorage Provisions.

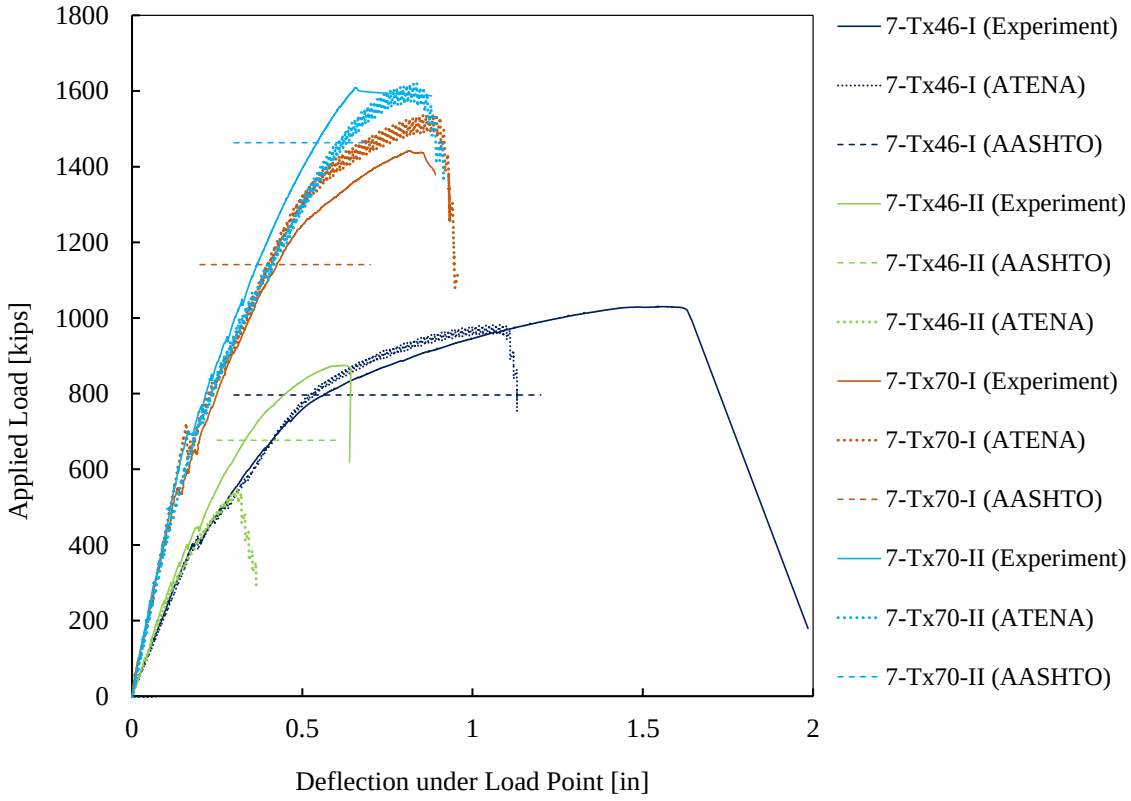

Force (kips) · 4.45 = force (kN); deflection (in.) · 2.54 = deflection (cm).

Figure 3.22: Shear tests of Tx-Girders with 0.7-in. (17.8-mm) diameter strands

Table 3.8: Comparison of calculated and measured load-carrying capacities

Specimen	Measured [kips (kN)]	AASHTO [kips (kN)]	ATENA [kips (kN)]
7-Tx46-I	1,029 (4,577)	843 (3,749)	982 (4,367)
7-Tx46-II	873 (3,883)	798 (3,549)	550 (2,447)
7-Tx70-I	1,436 (6,388)	1,101 (4,899)	1,538 (6,843)
7-Tx70-II	1,609 (7,157)	1,424 (6,333)	1,621 (7,209)

Figure 3.23 compares the experimental values against the ATENA and AASHTO estimated shear capacities. AASHTO predictions were conservative with a minimum ratio of 1.1 with respect to the measured capacities. ATENA predictions were within 10 % of the measured capacities with the exception of 7-Tx46-II. The poor estimate of this particular specimen may have resulted from excessive numerical bond slip caused by the large magnitude of bursting force at a relatively low concrete strength. Table 3.9 includes a list of the modeled specimens with the largest prestressing forces. 7-Tx46-II was tested at a concrete compressive strength of 6.9 ksi (48 MPa) with 1,786 kips (7,945 kN) of prestressing force. All other specimens were tested at greater concrete compressive strengths.

Table 3.9: Comparison of prestressing force relative to concrete compressive strength

Specimen ID	Applied Prestressing Force [kips (kN)]	Test-day f'_c [ksi (MPa)]
7-Tx46-II	1,786 (7,945)	6.9 (48)
6-Tx46-I	1,954 (8,690)	13.2 (91)
7-NU1100	2,025 (9,008)	10 (69)
7-Tx70-II	2,501 (11,123)	12.7 (88)

The mesh size in all specimens was 2 in. (50 mm) which is equal to the strand spacing. It is possible that the relatively low concrete strength subjected to such great

bursting stress within a single finite element may have contributed to numerical instabilities. The slip measurements obtained from 7-Tx46-II support this explanation. The numerical slip of 7-Tx46-II was 0.08 in. (2.01 mm) compared to the experimentally measured maximum slip of 0.07 in. (1.78 mm) at a peak applied load that is approximately 60 % greater than the numerically estimated peak load. Mesh refinement at the level of strands may help improve the numerical stability of the analysis.

All specimens demonstrated signs of anchorage distress and horizontal cracks along the web and flange interface; however, stirrup yielding was observed in all and AASHTO provisions conservatively estimated the capacities.

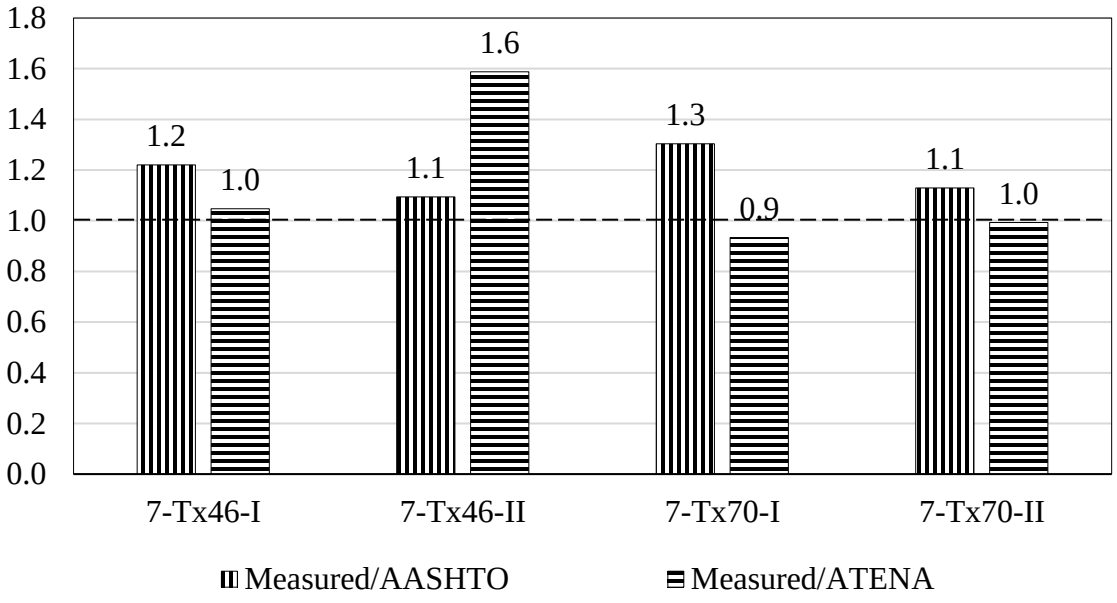

Figure 3.23: Ratio of measured to calculated load-carrying capacity of 7-Tx-Girders

Slip was monitored experimentally in the specimens. Table 3.10 lists the maximum strand slip at the peak load at each end of the Tx-Girders and compares them with the maximum predicted slips estimated by ATENA. Only halves of the first two specimens

were modeled and live and dead end slips could not be distinguished. The ATENA slip prediction is the overall maximum observed in a specimen. The strands seem to slip more at the dead end which may be attributed to the greater concrete damage and loss of bond. The release cracks formed in 7-Tx46-I were more severe than in 7-Tx46-II. The greater concrete damage may have led to the larger dead end slip in 7-Tx46-I compared with 7-Tx46-II. Figure 3.24 to Figure 3.27 compares the concrete damage observed at failure with the computed crack patterns.

Table 3.10: Strand slips at shear capacity of Tx-Girders with 0.7-in. (17.8-mm) diameter strands

Specimen	Measured [in. (mm)]		ATENA [in. (mm)]
	Live End	Dead End	
7-Tx46-I	0.05 (1.27)	0.15 (3.81)	0.09 (2.34)
7-Tx46-II	0.06 (1.52)	0.07 (1.78)	0.08 (2.01)
7-Tx70-I	0.05 (1.27)	0.01 (0.25)	0.06 (1.56)
7-Tx70-II	0.12 (2.97)	0.05 (1.20)	0.02 (0.43)

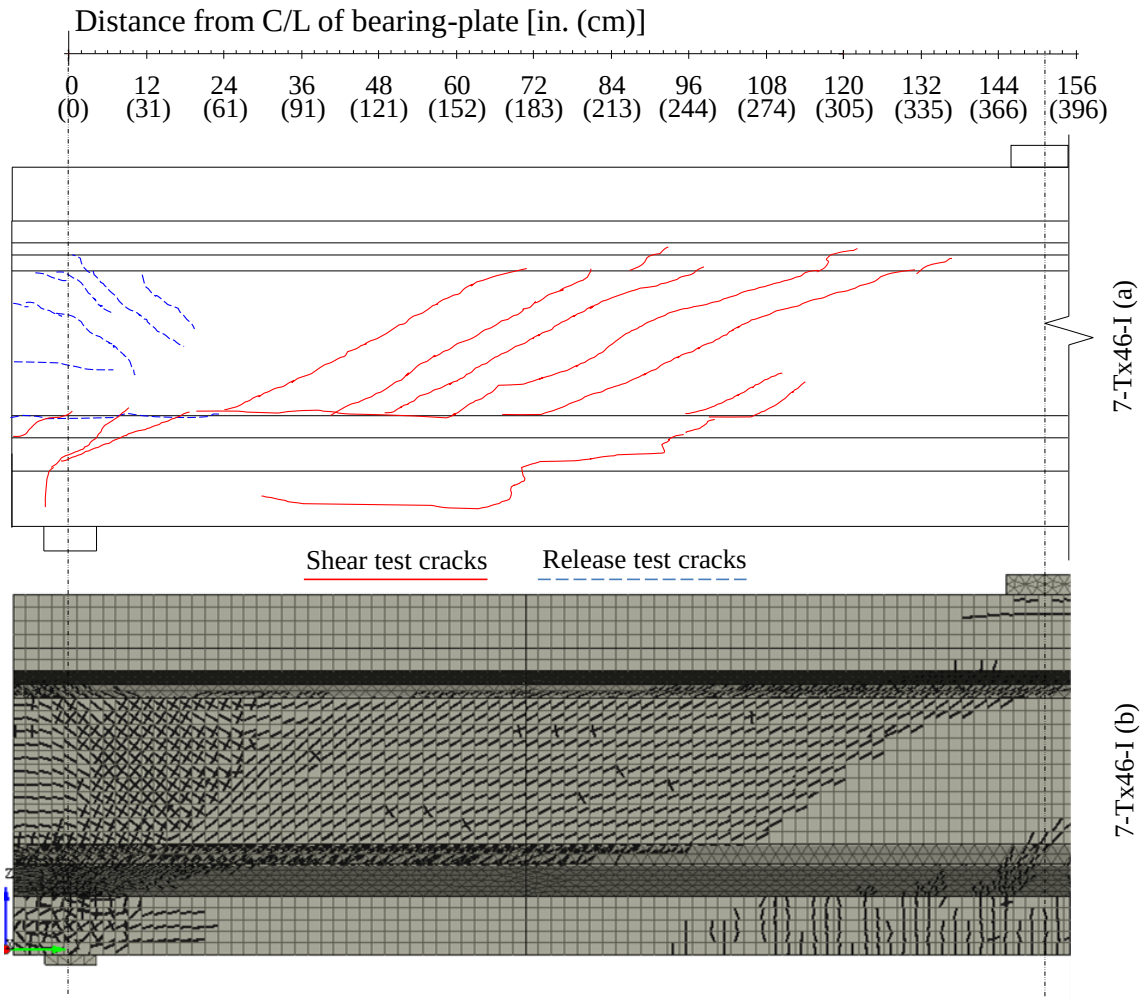

Figure 3.24: Shear test damage in 7-Tx46-I (a) experiment (b) ATENA

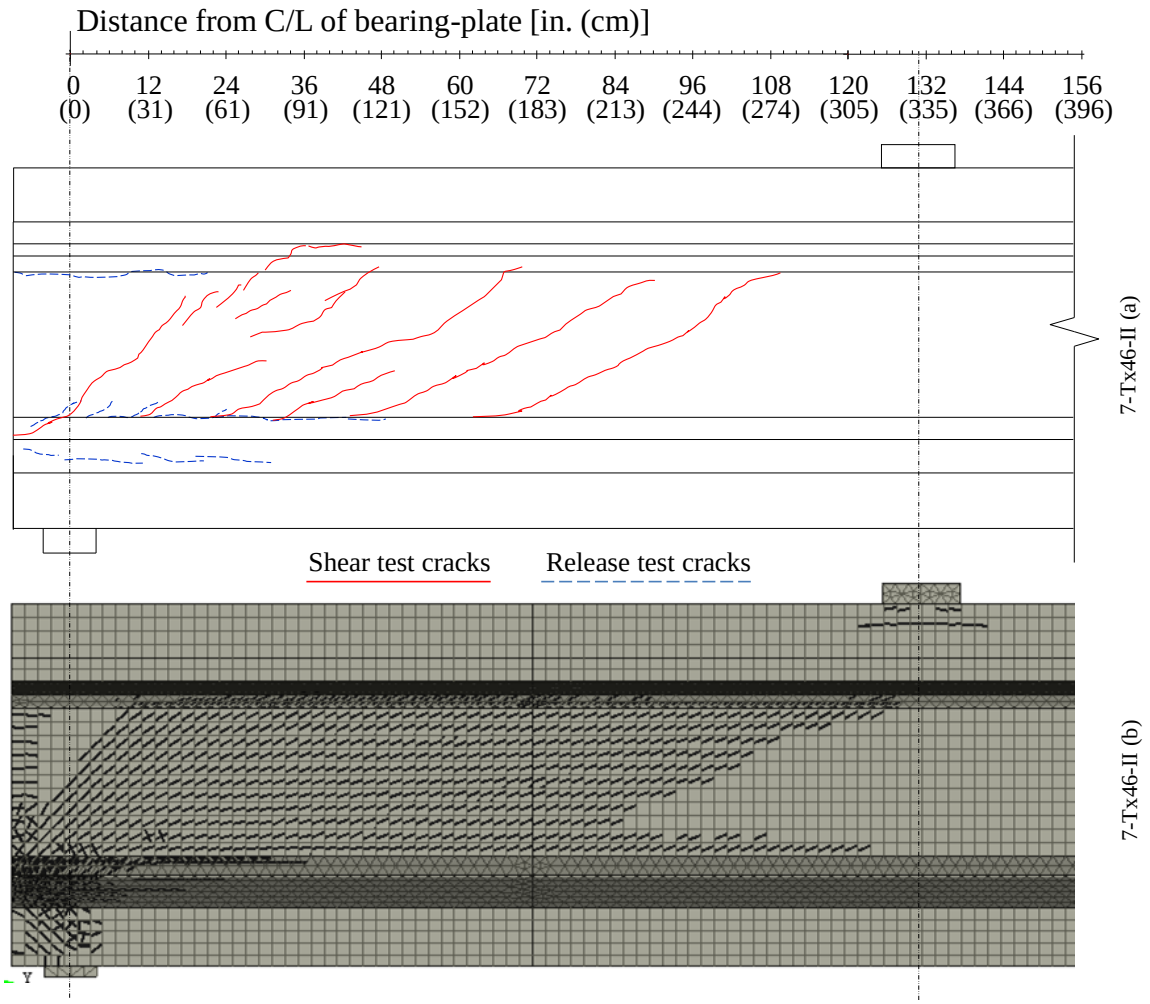

Figure 3.25: Shear test damage in 7-Tx46-II (a) experiment (b) ATENA

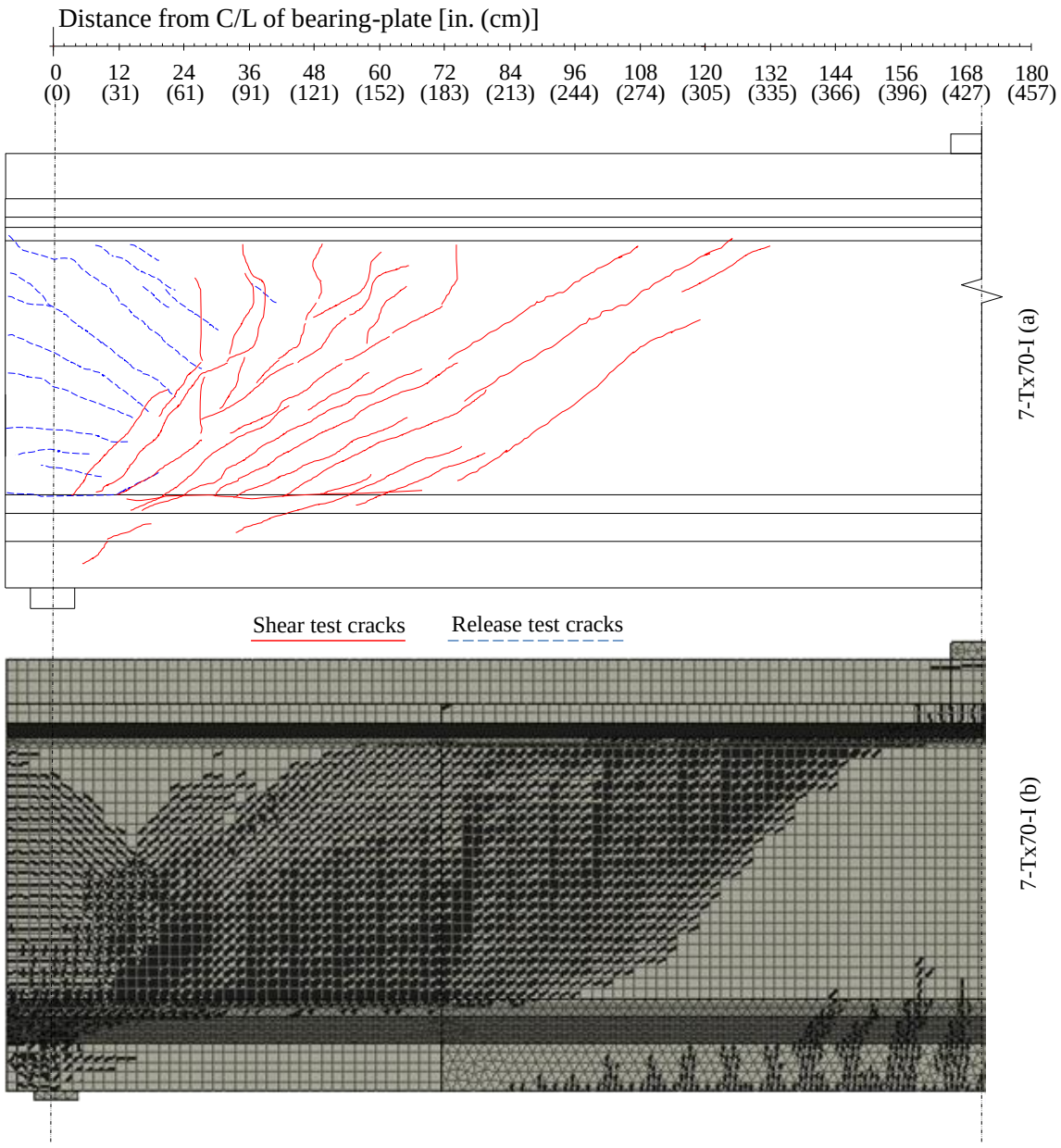

Figure 3.26: Shear test damage in 7-Tx70-I (a) experiment (b) ATENA

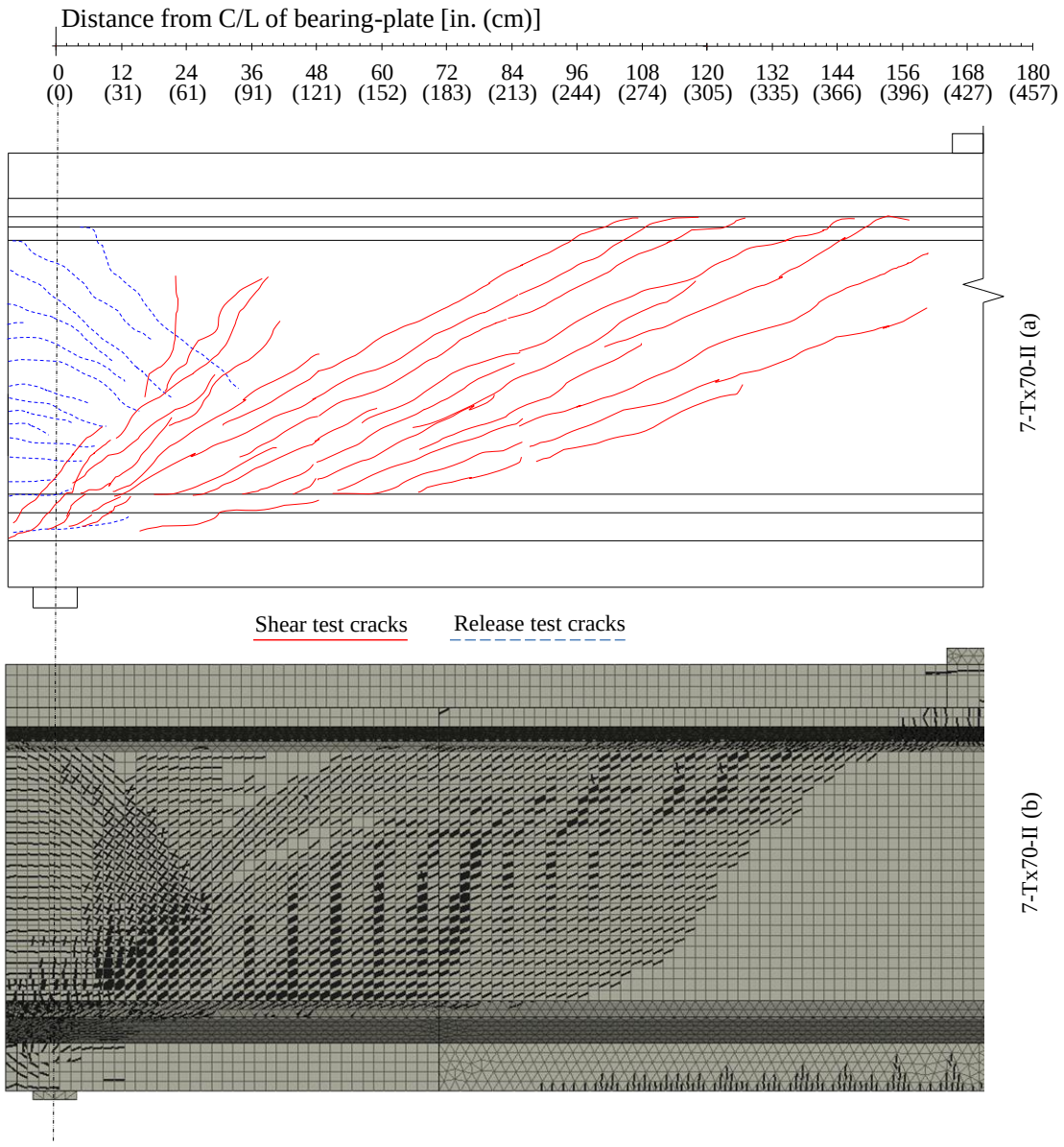

Figure 3.27: Shear test damage in 7-Tx70-II (a) experiment (b) ATENA

3.5 SUMMARY

ATENA was shown to be a reliable tool for predicting the failure modes of Tx-Girders with 0.7-in. (17.8-mm) diameter strands and the distribution of end-region damage at prestress transfer. While observed shear failure modes demonstrated signs of anchorage damage and horizontal cracking at web/flange interfaces, the specimen capacities were numerically estimated to be within 10 % of the measured capacities with the exception of 7-Tx46-II. As described earlier, this particular specimen was tested at a relatively low concrete compressive strength with large prestressing force magnitude. Numerical instabilities caused by excessive strand slip resulted in premature failure. Other essential findings were that the stiffness of the specimen and concrete cracking load which are automatically calculated as a function of user-input strength were captured for most specimens.

4. End-Region Investigation

With the aid of FEA and data obtained from the release test instrumentation, the performance of the standard Tx-Girder end-region reinforcement details was assessed. End-region concrete damage and reinforcement stresses were computed using ATENA and verified based on observations from seven Tx-Girder specimens (three with 0.6-in. (15.2-mm) strands and four with 0.7-in. (17.8-mm) diameter strands).

Firstly, the current end-region serviceability requirements are introduced. The function of the end-region reinforcement in Tx-Girders and observations about their effectiveness in controlling damage and stirrup stresses are described. The end-region reinforcement design of NU-Girders is briefly investigated for comparison with that of Tx-Girders. NU-Girders with 0.7-in. (17.8-mm) diameter strands have been employed in the field on the basis of the findings reported by Tadros & Morcous (2011). For the purpose of reducing typical damage and stirrup stresses, a number of reinforcement modifications in Tx-Girders are considered. The numerically-estimated results from incorporating additional end-region reinforcement of Tx-Girders with 0.7-in. (17.8-mm) diameter strands are discussed and recommendations regarding the most effective modification are provided.

4.1 Permissible End-Region Cracking

Cracking in the end-region of prestressed girders has long been a durability concern. Research has not been conducted on the correlation between end-region cracking and reinforcement corrosion, and in general, less in-depth research has been performed on end-region cracking than flexural cracking. A number of guidelines are available that provide limits for tolerable crack widths in RC members. Nawy has summarized tolerable

flexural crack widths from various sources in a 1968 ACI Journal article (Nawy, 1968). The ACI 224 report, "Control of Cracking in Concrete Structures", recognizes bursting cracks specific to prestressed girders; however, does not specifically address them. Instead, it provides a generalized limit for crack widths based on the severity of the environmental conditions. The 2006 PCI manual, "Manual for the Evaluation and Repair of Precast, Prestressed Concrete Bridge Products", is more direct in specification of tolerable limits for end-region cracking. The 2014 TxDOT manual, "Standard Specifications for Construction and Maintenance of Highways, Streets, and Bridges" specifies only the following regarding end-region crack in prestressed I-girders.

> *"Seal cracks in I-beam ends exceeding 0.005 in. in width as directed. The fabricator must decrease the spacing of Bars R and S in I-beam by providing additional bars to help limit crack width. No less than 1 in. clearance between bars will be permitted. The fabricator must take approved corrective actions if cracks greater than 0.005 in. form. All work, material, and engineering related to these cracks will be at the Contractor's expense." (TxDOT, 2014)*

As evident from Table 4.1, TxDOT has the smallest tolerable crack width limit at 0.005-in. (0.13 mm). Given the average annual humidity of 64 % in the state of Texas, and the mild use of de-icing agents, crack widths up to 0.008-0.012 in. (0.20-0.31 mm) are tolerated according to the other listed sources in Table 4.1. Based on the non-TxDOT limits, all Tx-Girders with 0.7-in. (17.8-mm) diameter strands would be assessed as having adequate crack control performance immediately following release. Based on conversations with TxDOT, end-region crack widths in Tx-Girders with 0.6-in. (15.2-mm) diameter strands are typically 0.005 in. (0.13 mm) or less. Given the effects of creep and

shrinkage, the cracks are expected to grow with time up to deck placement. TxDOT has expressed potential concerns about intolerable crack widths prior to deck placement which may take place six months up to one year after cast. The remainder of this chapter focuses on investigating constructible modifications that contribute to crack width reduction.

Table 4.1: Summary of tolerable crack widths (adapted from Hasenkamp (2008))

Source	Exposure Condition	Tolerable Crack Width [in. (mm)]	
Brice (1958)	Severe	0.004 (0.10)	
	Aggressive	0.008 (0.20)	
	Normal	0.012 (0.30)	
Rusch (1958)	Aggressive (salt-water)	0.008 (0.20)	
	Normal	0.012 (0.30)	
Etsen (1958)	Severe to Aggressive	0.002-0.006 (0.05-0.15)	
	Normal (outside)	0.006-0.010 (0.15-0.25)	
	Normal (inside)	0.010-0.014 (0.25-0.36)	
ACI 318-63 (1963)	Exterior	0.010 (0.25)	
	Interior	0.015 (0.38)	
CEB (1964)	Interior or exterior (aggressive & water tight)	0.004 (0.10)	
	Aggressive	0.008 (0.20)	
	Normal	0.012 (0.30)	
US Bureau of Public Roads (1966)[1]	Load Type	Case 1[2]	Case 2
	Air or protective membrane	0.012 (0.30)	0.010 (0.25)
	Salt, air, water & soil	0.010 (0.25)	0.008 (0.20)
	De-icing chemicals, humidity	0.008 (0.20)	0.006 (0.15)
	Seawater & seawater spray, alternate wetting & drying	0.008 (0.20)	0.006 (0.15)
ACI 224R-01 (2003)	Dry air or protective membrane	0.016 (0.41)	
	Humidity, moist air, soil	0.012 (0.30)	
	De-icing chemicals	0.007 (0.18)	
	Seawater & seawater spray, wetting & drying	0.006 (0.15)	
	Water-retaining structures (excluding non-pressure pipes)	0.004 (0.10)	
PCI MNL-37-06 (2006)	Humidity	≤0.012 (0.30)	
	De-icing chemicals	≤0.007 (0.18)	
	Seawater & seawater spray, wetting & drying	≤0.006 (0.15)	
TxDOT (2014)	All conditions	≤0.005 (0.13)	

[1] Maximum crack width at street level under service load
[2] Case 1: Dead load causes compression and live load causes tension. Case 2: both cause tension.

4.2 TX-GIRDER END-REGION REINFORCEMENT

Tx-Girders contain four specific end-region reinforcing bars. The girders are designed based on AASHTO LRFD Section 5.10.10.1 (AASHTO, 2014) for "splitting resistance of pretensioned anchorage zones". AASHTO specifies that the splitting resistance, P_r, provided by the total area of reinforcement at a distance of $h/4$ from the end of the beam must resist at least 4 % of the total prestressing force in the girder and the stress in the reinforcement, f_s, must not exceed 20 ksi (138 MPa) as shown in the following equation.

$$P_r = f_s \cdot A_s \qquad \text{Equation 4.1}$$

AASHTO also notes the following:

- Reinforcement used to satisfy this requirement can also be used to satisfy other design requirements.
- The reinforcement shall be as close to the end of the beam as practicable.
- The 20 ksi (138 MPa) stress limit in this provision is for crack control. This level of stress corresponds to a tolerable crack width.
- In addition to spalling (or splitting) reinforcement, AASHTO specifies confinement reinforcement comprised of at least No.3 deformed bars at 6-in. (15-cm) spacing for a length of $1.5 \cdot d$ to enclose the bottom flange strands.

Figure 4.1 demonstrates the dimensions and spacing of the current Tx-Girder end-region reinforcing bars. C- and U-Bars provide confinement within the bottom flange, and S- and R-Bars contribute to splitting resistance in the end-region.

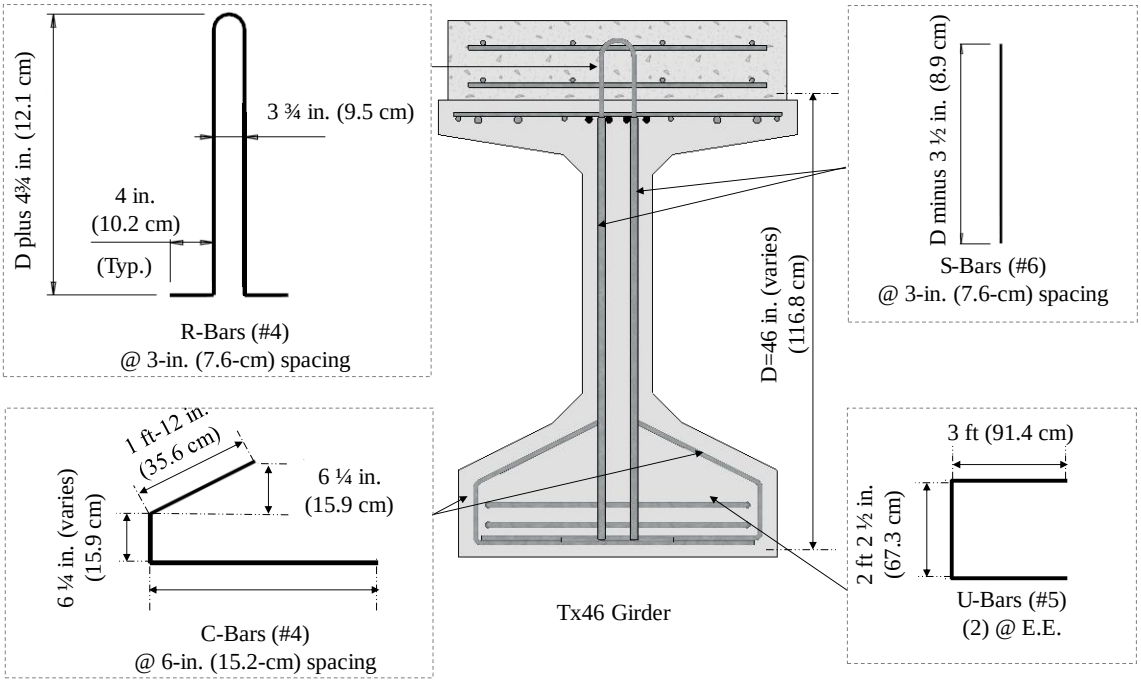

Figure 4.1: Tx-Girder end-region reinforcing details. This spacing continues for 3 ft (914 mm) at each end.

To characterize the intensity of spalling stresses in a specimen as a function of strand eccentricity relative to section depth and bursting forces, factor, α has been defined as follows:

$$\alpha = \left(A_{ps} \cdot f_{pi} \cdot \frac{e_{ps}}{y_{bot}}\right)_{Bottom\ Strands} \qquad \text{Equation 4.2}$$

α permits comparison of end-region stress intensity among girders of various depths. The following table reiterates the performance of the 7-Tx-Girders in relation to the intensity factor α. The crack width and reinforcement stresses shown in Table 4.2 are measurements obtained from the experiment corresponding to the time immediately following prestress transfer.

Table 4.2: Relation between α and measured end-region performance of Tx-Girders with 0.7-in. (17.8-mm) diameter strands

Specimen	α [kips (kN)]	w_{crack} max. [in. (mm)]	$\sigma_{s,max}$ [ksi (MPa)]
7-Tx46-I	1,202 (5,347)	0.008 (0.2)	19 (131)
7-Tx46-II	860 (3,826)	0.004 (0.1)	14 (97)
7-Tx70-I	1,478 (6,575)	0.006 (0.15)	25 (172)
7-Tx70-II	2,157 (9,595)	0.007 (0.18)	26 (179)

The maximum stresses measured in the specimens are larger for specimens with higher α factors. Similarly, the crack widths increase proportionally to α (with the exception of 7-Tx46-I where a crack width of 0.008 in. (0.2 mm) was observed over a short length). The measured stresses exceed 20 ksi (138 MPa) for both 7-Tx70-I and 7-Tx70-II. Further, the crack widths are larger than the TxDOT limit in all cases except for 7-Tx46-II. Therefore, there is a need to better control cracks and further reduce reinforcement stresses.

4.3 NDOR End-Region Reinforcement

As NU-Girders are already being manufactured with 0.7-in. (17.8-mm) diameter strands, it is useful to also examine their performance. The primary differences between Tx-Girders and NU-Girders in terms of bursting and spalling reinforcement are:

- Unlike in Tx-Girders, the bursting reinforcement in NU-Girders fully enclose the bottom flange strands. A model of 7-Tx46-I with fully closed C-Bars did not indicate any serviceability improvements.
- Area of spalling reinforcement in NU-Girders does not meet AASHTO and is less than in 7-Tx46-I (strand force in the NU1100 girders is 33 % greater than in 7-Tx46-I).

Table 4.3 and Table 4.4 summarize the amount of bursting and spalling reinforcement, respectively, in the NU1100 girders and 7-Tx46-I girder. The two specimens are compared as specimens with similar depths (Tx46 is 46-in. (1.17-m) and NU1100 is 43-in. (1.1-m) deep). In Table 4.3, the bursting reinforcement in the NU-Girders is compared with 7-Tx46-I in terms of area of bursting reinforcement per unit length into the $1.5 \cdot d$ region. Cap bar reinforcement area is shown as a component of the reinforcement area; however, the cap bar effect should be considered in terms of provision of confinement rather than added bursting steel area.

Table 4.3: Comparison of bursting reinforcement requirements (area of reinforcement per unit length over $1.5 \cdot d$)

Specimen	$1.5 \cdot d$ [in. (cm)]	Standard	As-Built [in.^{2}/ft (mm^2/cm)]	
			Bar	Cap Bar
7-Tx46-I[1]	76 (195)	TxDOT	0.86 (219)	-
NU1100-I	72 (182)	NDOR BOPP	0.25 (64)	0.26 (65)
NU1100-II		AASHTO	0.48 (121)	0.48 (121)
NU1100-III		NDOR BOPP + AASHTO	0.48 (121)	0.48 (121)

[1] No.4 @ 6 in. (15 cm) for 76 in. (195 cm)

The bursting reinforcement specified by TxDOT provides more confinement than present in NU-Girders. Given that the cap bar in NU-Girders is spaced at 12 in. (31 cm), the confinement reinforcing bars do not always fully enclose the strands.

The spalling reinforcement area, A_s, listed in Table 4.4 corresponds to the total area of vertical reinforcement within a distance $h/4$ from the end face of each specimen. As shown, the spalling reinforcement of NU1100 girders with the total prestressing force does not meet the AASHTO requirements. However eight strands are debonded only at one end of the specimen which reduces end-region stresses at that end. If the prestressing force

from debonding of eight strands is deducted from the total prestressing force in the end-region, the AASHTO requirement for spalling reinforcement reduces to 3.52 in^2 (22.7 cm^2). Subsequently, the provided NU1100 reinforcement meets AASHTO requirement for spalling reinforcement at the debonded end.

Table 4.4: Comparison of spalling reinforcement requirements

Specimen	Total P/S Force [kips (kN)]	Bottom strands eccentricity, e_{ps} [in. (cm)]	A_s [in.^{2} (cm^2)]		
			TxDOT	AASHTO	NDOR BOPP
7-Tx46-I	1,614 (7,179)	16.8 (42.7)	5.12 (33.0)	3.40 (21.9)	N/A
NU1100-I[1]	2,148 (9,555)	16.6 (42.2)	N/A	4.52 (29.2)	3.77 (24.3)

[1] The same requirement applies to NU1100-II and NU1100-III since they have the same prestressing force, vertical reinforcement (including coil rods) and overall section depth.

Tadors & Morcous (2011) did not comment on the end-zone cracks; however, release models of the NU1100 girders predicted the following results in relation with α, immediately following prestress transfer (Table 4.5). It is important to note that the end with debonded strands experienced less damage (40 % reduction in the maximum web crack width at the debonded end) and reduced transverse/confining reinforcement stresses.

Table 4.5: Relation between α and performance in NU-Girders with 0.7-in. (17.8-mm) diameter strands

Specimen	α [kips (kN)]	w_{crack} max. [in. (mm)]	$\sigma_{s,max}$ [ksi (MPa)]
7-NU1100-I	1,715 (7,629)	0.010 (0.24)	38 (262)
7-NU1100-II		0.014 (0.35)	39 (267)
7-NU1100-III		0.010 (0.26)	40 (272)

Given that α of NU-Girders is less than 7-Tx70-II and both specimens have similar concrete release strengths (7.8 ksi (53.8 MPa) for NU-Girders versus 8.0 ksi (55 MPa) for 7-Tx70-II), smaller stresses and crack widths could be anticipated in the NU-Girders. However, as a result of the smaller area of spalling steel provided in the NU-Girders, greater end-region damage and reinforcing bar stress estimates were obtained.

4.4 FEA OF CURRENT TX-GIRDER REINFORCEMENT

ATENA predictions were shown to capture the variation in concrete damage and reinforcement stresses relative to the intensity factor with reasonable levels of accuracy for the Tx-Girders. The assessments presented hereafter are based on FEA results (Table 4.6) performed in a similar manner as discussed in Chapter 2. Results in the following table correspond to damage estimates immediately following prestress transfer and presents the computed stresses in S-, R-, C-, and U-Bars. It is important to note that the maximum stresses in the R- and S-Bars correspond were estimated to occur within very small localized regions (i.e., within one finite element per bar).

Table 4.6: Relation between α and FEA of Tx-Girders with 0.7-in. (17.8-mm) diameter strands

Specimen	α [kips (kN)]	Max stress [ksi (MPa)]				Max crack [in. (m)]
		S	R	U	C	
7-Tx46-I	1,202 (5,347)	23 (158)	22 (153)	-25 (-173)	7 (50)	0.007 (0.17)
7-Tx46-II	860 (3,826)	10 (66)	9 (64)	-19 (-129)	9 (65)	0.004 (0.11)
7-Tx70-I	1,478 (6,575)	21 (147)	25 (175)	-20 (-138)	7 (50)	0.007 (0.18)
7-Tx70-II	2,157 (9,595)	26 (181)	32 (218)	-28 (-196)	10 (66)	0.009 (0.23)

From the analyses performed, it was estimated that:

- In specimens with large prestress eccentricities, the maximum stresses were generated closer to the end face and a greater number of cracks were distributed along the height of the web near the end face.
- In specimens with smaller eccentricities (the centroid of prestressing force is closer to the bottom flange-web interface), the largest stresses formed farther away from the end face of the beam (1 ft (305 mm) or more).
- Using C-Bars to fully enclose the strands had little impact on estimated damage.
- Stresses in all the end-region reinforcing bars (except for U-Bars) were numerically estimated to decrease with time following prestress transfer.

4.5 FEA OF RECOMMENDED TX-GIRDER REINFORCEMENT

Three reinforcement design detailing alternatives were investigated as potential modifications to the standard end-region detailing of Tx-Girders. Figure 4.2 illustrates schematics of the three alternatives considered. The modifications are described as follows:

- I-Bar: Placement of four vertical No.6 bars at each end of the specimen similar to the "coil rods" in NU-Girders.
- Modified S-Bar: Replacement of the first four pairs (eight units) of No.6 S-Bars with No.8 S-Bars at each end.
- W-Bar: Placement of horizontal No.4 bars along the height of the web up to 3 ft (91 cm) into the beam and at 5-in. (13-cm) spacing. The bars will be tied to the interior of the S- and R-Bars.

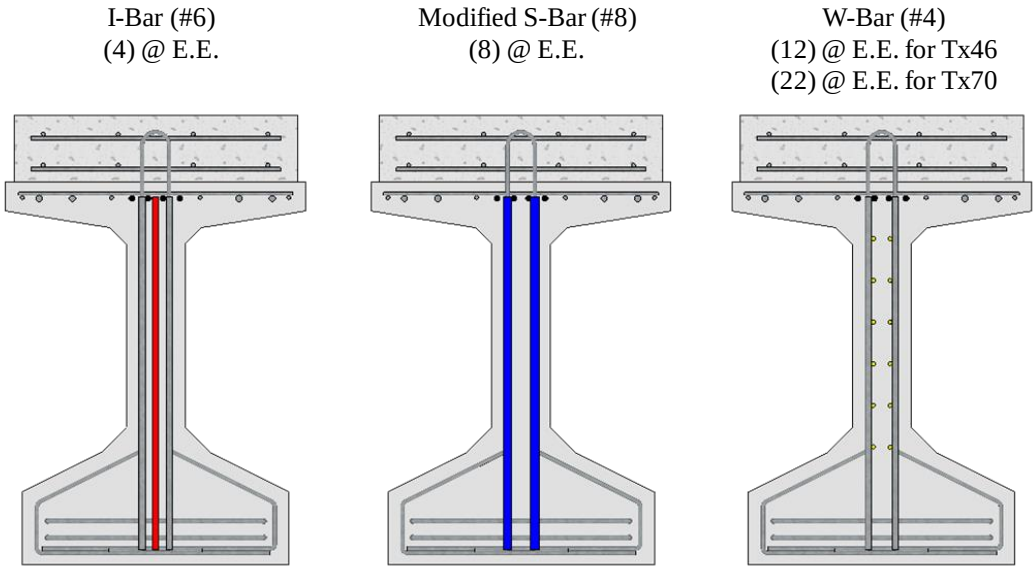

	Additional weight:		
(Tx46)	45 lbs (21 kg)	69 lbs (31 kg)	48 lbs (22 kg)
(Tx70)	69 lbs (31 kg)	107 lbs (49 kg)	88 lbs (40 kg)

Figure 4.2: Schematic of recommended reinforcement modifications

Each of the three alternatives was modeled independently in the four 7-Tx-Girders resulting in twelve models. End-region responses were measured in each of the models and compared with the control specimens which consisted of standard TxDOT reinforcement detailing. The percent change in each measure of serviceability was divided by the added weight of steel required by the specific detail. The greatest effect was produced by the "Modified S-Bar" option. Figure 4.3 demonstrates the performance of each alternative in terms of reduction in overall maximum and maximum web crack widths and vertical reinforcement stresses. All measurements correspond to the time after the application of deck self-weight and girder-only shrinkage (see Chapter 2) representing at least 28 days after cast to account for shrinkage-induced cracks.

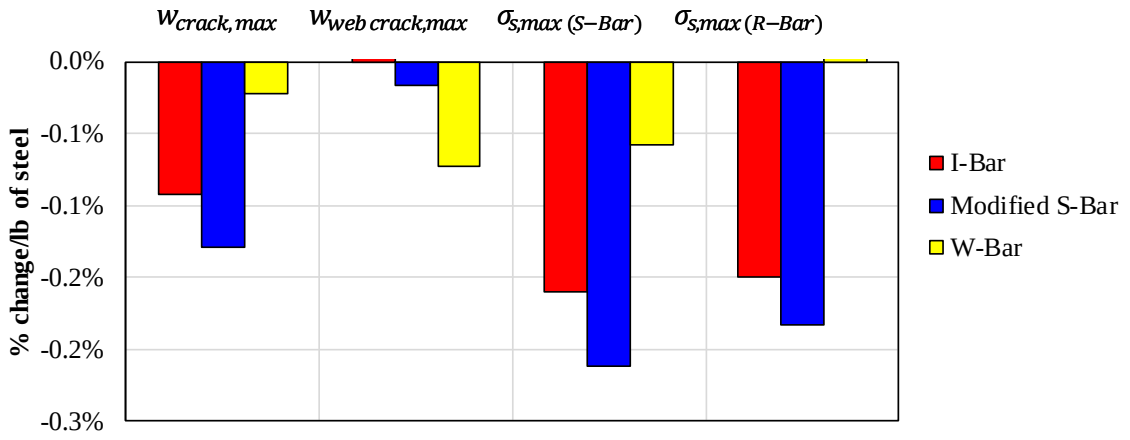

Figure 4.3: Effectiveness of reinforcement modification in reduction of end-region crack width or reinforcement stresses normalized by added weight of steel

Increasing the diameter of the first 8 S-Bars from No.6 to No.8 bars, is the most effective option, but also the heaviest option in terms of added steel. Based on the author's experience in fabricating the reinforcing cage for the specimens, this modification is almost negligible in terms of change in construction time and effort. W-Bars are especially helpful in reducing the maximum crack width observed along the web height only; however, not the overall maximum crack width. Web crack widths are easily identifiable, but they are typically less critical than cracks in the flanges and near the strands.

5. Conclusions

A uniform modeling procedure comprised of modeling assumptions, definition of boundary conditions, material properties and load conditions representing the actual loads on prestressed concrete I-girders was developed using ATENA 3D.

The modeling approach was validated with actual experimental data obtained from seven release tests, and ten shear-critical load tests. The validated finite element modeling procedure was employed to investigate the effects of three alternative reinforcement detail modifications on four different I-girder specimens resulting in a sample size of twelve. The specimens consisted of different degrees of eccentricity, and intensity of bursting and spalling stresses. All specimens were modeled with 0.7-in. (17.8-mm) diameter strands to specifically focus these efforts on the end-region serviceability of I-girders fabricated with larger diameter 0.7-in. (17.8-mm) diameter strands.

The numerical model allowed for observations that are not easily achieved by experimental testing such as determining the trend of stress distribution in end-region reinforcing bars as a function of strand eccentricity. Observations made based on the validated models are introduced first, followed by recommended reinforcement modifications for the reduction of end-region damage.

Findings on prestress transfer:

- In specimens with large strand eccentricities, the maximum stirrup stress was estimated to develop near the end-faces. In specimens with greater bursting forces, the maximum stirrup stress was shown to develop approximately 15 to 20 in. (380 to 510 mm) into the beam. In both cases,

the maximum stresses were estimated to develop near the strands, closer to the bottom flange, and the stresses dissipated with distance from strands.

- Numerically estimated crack widths immediately following release did not exceed 0.009 in. (0.23 mm). This level of cracking will require repair according to existing TxDOT standards, but is considered acceptable according to other sources and accounting for the weather and road conditions in Texas.
- Computed crack widths were observed to grow in width and length with time as a function of concrete shrinkage and creep. The crack widths were estimated to vary based on the applied numerical shrinkage (or how long the specimens are stored prior to deck placement).
- Reinforcement stresses which are an indication of level of concrete cracking were estimated to be, on occasion, larger than the 20 ksi (138 MPa) limit specified by AASHTO; however, these stresses were estimated to reduce with time as concrete crack widths grew.

Findings on end-region crack control:

- The numerical modeling of the alternative reinforcement details indicated that replacing the first eight (No.6) S-Bars with No.8 bars at each end results in the largest reductions in computed crack widths and steel stresses. This option also requires 69 lbs (31 kg) and 107 lbs (49 kg) of added steel for Tx46 and Tx70 girders, respectively. The construction time and effort implications are believed to be negligible.

- Combing horizontal and vertical end-region reinforcing bars (W-Bars and I-Bars) was shown to result in a significant and more effective reduction in end-region damage.

6. Future Research

To ensure the adequacy of the recommended end-region reinforcement modification, it is recommended that experimental testing be conducted in a series of I-girder specimens with different designs (i.e., different levels of bursting and spalling stresses).

To accurately model the growth of cracks with time and better address the serviceability issues found in prestressed girders prior to deck placement, it is essential to conduct a survey through which crack growth is monitored over time in prestressed girders fabricated in various plants. The crack widths should be monitored from the day of girder casting to when the bridge is in service. Such a survey will accommodate the development of a more reliable time-dependent FEM of the end-region.

It is recommended to place VWG inside the monitored specimens to obtain an accurate measurement of the prestress losses. A database of monitored prestress loss histories as a function of shrinkage and creep will significantly improve the accuracy of the numerical estimations.

Appendix

The following tables summarize whether the Tx-Girders with 0.6-in. (15.2-mm) strands satisfied the spalling and bursting reinforcement requirements. Bursting reinforcement requirements were not satisfied for CEB-FIP MC 90 and the other two provisions did not have specific bursting reinforcement requirements. Spalling reinforcement requirements are met according to all except for AASHTO (2007) provisions. The spalling reinforcement area used in this assessment includes the shear reinforcement in the end-region as well as the spalling-specific No. 6 bars.

Table A. 1: 6-Tx28-I and 6-Tx28-II end-region reinforcement design (O'Callaghan, 2007)

6-Tx28-I and 6-Tx28-II	Spalling Reinforcement		Bursting Reinforcement	
	Live End	Dead End	Live End	Dead End
AASHTO (2007)	N	N	N/A	N/A
PCI (6th Ed.)	Y	Y	N/A	N/A
CEB-FIP MC 90	Y	Y	N	N

Table A. 2: 6-Tx46-I end-region reinforcement design (O'Callaghan, 2007)

6-Tx46-I	Spalling Reinforcement		Bursting Reinforcement	
	Live End	Dead End	Live End	Dead End
AASHTO (2007)	N	Y	N/A	N/A
PCI (6th Ed.)	Y	Y	N/A	N/A
CEB-FIP MC 90	Y	Y	N	N

Glossary

a	Test span length [ft (m)]
A_s	Total area of vertical reinforcement at a distance $h/4$ from the end of the beam [in.^{2} (m^2)]
A_{ps}	Total area of strands [in.^{2} [cm^2)]
BOPP	Bridge Operations, Policy, and Procedure
C/L	Centerline
d	Distance from compression face to centroid of reinforcement [in. (cm)]
d_p	Distance from the topmost compression fiber to the centroid of prestressing reinforcement [in. (cm)]
D_b	Strand nominal diameter [in. (cm)]
E	ATENA notation for concrete elastic modulus [ksi (MPa)]
E.E.	Each end
E_p	Strand young's modulus [ksi (MPa)]
e_{ps}	Distance measured from the geometric centroid of the girder (excluding the deck) to the centroid of the prestressing reinforcement [in. (cm)]
f'_c	Concrete compressive strength at release [ksi (MPa)]
f'_{ci}	Concrete compressive strength at release [ksi (MPa)]
f_{pi}	Strand stress prior to casting [ksi (MPa)]
f_s	Stress in the vertical reinforcement at a distance $h/4$ from the end of the beam [ksi (MPa)]
f'_t	Concrete tensile strength [ksi (MPa)]
F_y	Yield strength [ksi (MPa)]
F_u	Rupture strength [ksi (MPa)]
G_F	ATENA notation for concrete specific fracture energy

h	Overall dimensions of the precast member in the direction in which splitting resistance is being evaluated [in (cm)]
L_t	Prestressing strand transfer length [in. (cm)]
NDOR	Nebraska Department of Roads
$P_{Flexure}$	The total nominal capacity of the specimen governed by flexural failure [kips (kN)]
P_{Shear}	The total nominal capacity of the specimen governed by shear failure [kips (kN)]
P_r	Splitting resistance [kips (kN)]
R	Remaining stirrups
s_{max}	ATENA notation for crack spacing
Span Length	The measured distance between the centerlines of the bearing-plates
Strds.	Strands
$w_{crack,max}$	Maximum crack width observed on the specimen surface [in (mm)]
W_d	ATENA notation for concrete critical compressive displacement
$w_{web\ crack,max}$	Maximum crack width in the web of the I-girder [in (mm)]
α	Spalling stress intensity factor [kips (kN)]
β	ATENA notation for concrete multiplier for the plastic flow direction
ε_{cp}	ATENA notation for concrete plastic strain at compressive strength
ε_{lim}	ATENA notation for steel strain at rupture
ε_{sh}	ATENA notation for steel strain at the unset of strain hardening
ε_u	ATENA notation for steel strain at the peak load
ε_y	ATENA notation for steel yield strain
μ	ATENA notation for concrete Poisson's ratio
ρ	ATENA notation for concrete specific material weight
$\sigma_{s,\max}$	The magnitude of the maximum measured stress in the No.4 stirrups [ksi (MPa)]
$\sigma_{s,\max(R-Bar)}$	Maximum stress in the end-region R-Bars [ksi (MPa)]

$\sigma_{s,\max(S-Bar)}$	Maximum stress in the end-region S-Bars [ksi (MPa)]
σ_t	ATENA notation for steel rupture strength [ksi (MPa)]
σ_y	ATENA notation for steel yield strength [ksi (MPa)]
φ	Resistance factor
$\#$	No. (reinforcing bar size)

References

AASHTO. (2014). *AASHTO LRFD Bridge Design Specifications, Seventh Edition.* American Association of State Highway and Transportation Officials (AASHTO).

ACI Committee 224. (2003). *Control of Cracking in Concrete Structures (ACI 224R-01).* Famington Hills: American Concrete Institute.

ACI Committee 318. (1963). *Building Code Requirements for Structural Concrete (ACI 318-63).* Farmington Hills: American Concrete Institute.

ACI Committee 318. (2014). *Buiding Code Requirements for Structural Concrete (ACI 318-04).* Farmington Hills: American Concrete Institute (ACI).

Amorn, W., Girgis, A., Bowers, J., & Tadros, M. (2007). Fatigue of Deformed Welded Wire Reinforcement. *PCI Journal*, 106-120.

Avendaño, A. (2008). *Shear Strength and Behavior of Prestressed Concrete Beams.* Austin: University of Texas at Austin.

Bigaj, A. J. (1999). *Structural Dependence of Rotations Capacity of Plastic Hinges in RC Beams and Slabs.* Delft: Delft University of Technology.

CEB. (1964). *Recommendation for an International Code of Practice for Reinforced Concrete.* Paris: Comite Europeen du Beton (CEB).

CEB. (1987). *Anchorage Zones of Prestressed Concrete Members, State-of-the-Art Report.* CEB Bulletin No. 181.

CEB-FIP. (1993). *CEB-FIP Model Code 1990.* London: Thomas Telford.

Červenka, V., & Červenka, J. (2015). Czeck Republic.

Garber, D. B. (2014). *Effect of New Prestress Loss Estimation Procedure on Prexast, Pretensioned Bridge Girders.* Austin: University of Texas at Austin.

Hasenkamp, C. J., Badie, S. S., Tuan, C. Y., & Tadros, M. K. (2008). *Sources of End Zone Cracking of Pretensioned Concrete Girders.* Lincoln: University of Nebraska-Lincoln.

Hovell, C., Avendaño, A., Moore, A., Dunkman, D., Bayrak, O., & Jirsa, J. (2012). *Structural Performance of Texas U-Beams at Prestress Transfer.* Austin: University of Texas at Austin Center for Transportation Research.

Hoyer, E., & Friedrich, E. (1939). Beitrag zur Frage der Haftspannung in Eisenbetonbauteilen [Contribution to the Question of Bond in Concrete Elements]. *Beton und Eisen, V.30*, 107-110.

Lenschow, R. J., & Sozen, M. A. (1965). Practical Analysis of the Anchorage Zone Problem in Prestressed Beams. *Journal of the American Concrete Institute, 62*, 1421-1438.

Nawy, E. G. (1968). Crack Control in Reinforced Concrete Structures. *ACI Journal*, 825-836.

O'Callaghan, M. (2007). *Tensile Stresses in the End Regions of Pretensioned I-Beams at Release.* Austin: University of Texas at Austin.

Okumus, P., & Oliva, M. G. (2013). Evaluation of Crack Control Methods for End Zone Cracking in Prestressed Concrete Bridge Girders. *PCI Journal*, 91-105.

Okumus, P., Kristam, R. P., & Arancibia, M. D. (2016). Sources of Crack Growth in Pretensioned Concrete-Bridge Girder Anchorage Zones after Detensioning. *Journal of Bridge Engineering*, 04016072-1-04016072-10.

Okumus, P., Oliva, M. G., & Becker, S. (2012). Nonlinear Finite Element Modeling of Cracking at Ends of Pretensioned Bridge Girders. *Engineering Structures*, 267-275.

Patzlaff, Q., Morcous, G., Hanna, K., & Tadros, M. (2012). Bottom Flange Confinement Reinforcement in Precast Prestressed Concrete Bridge Girders. *Journal of Bridge Engineering*, 607-616.

Paulet, E. G.; Bureau of Public Roads, Bridge Division. (1966). *Reinforced Concrete Bridge Members: Strength and Serviceability Criteria, Ultimate Design.* Washington: US Department of Commerce, Bureau of Public Roads.

PCI. (2006). *Manual for the Evaluation and Repair of Precast, Prestressed Concrete Bridge Products (MNL-37-06).* Chicago: PCI.

Pryl, D. (2015, November 20). (R. Abyaneh, Interviewer)

RILEM International Symposium on Bond and Crack Formulation in Reinforced Concrete (Stockholm 1957), V. 1-4. (1958). (p. 880). Stockholm: Tekniska Hogskolans Rotaprintryekeri.

Russell, B. W., & Burns, N. H. (1993). *Design Guidelines for Transfer, Development and Debonding of Large Diameter Seven Wire Strands in Pretensioned Concrete Girders.* Austin: The University of Texas at Austin Center for Transportation Research.

Schuler, G. (2009). Producer's Experience with 10,000 psi Concrete and 0.8-in. Diameter Strands. *HPC Bridge Views*, 9-11.

Tadros , M. K., & Morcous, G. (2011). *Impact of 0.7 inch Diameter Strands on NU I-Girders* . Lincoln: University of Nebraska-Lincoln.

TxDOT. (2014). *Standard Specifications for Construction and Maintenance of Highways, Streets, and Bridges.* Texas Department of Transportation.

TxDOT. (2015). *LRFD Bridge Design Manual.* Austin: TxDOT.

Vita

Roya Alirezaei Abyaneh was born in Tehran, Iran. She completed primary and middle school in Iran and high school in the UAE. Roya attended the University of Waterloo for undergraduate studies in Civil Engineering followed by Graduate Studies at the University of Texas at Austin. She now practices structural engineering and resides in Houston, Texas.

Permanent e-mail: Roya.Abyaneh@Hotmail.com

This thesis was typed by Roya Alirezaei Abyaneh.